UNIVERSITÀ POLITECNICA DELLE MARCHE

Facoltà di Medicina e Chirurgia

Tesi di Dottorato

Corso di Dottorato in Scienze Biomediche

XXXIV ciclo

Biomarkers of angiogenesis and clinical outcomes to Cabozantinib and Everolimus in Patients with Metastatic Renal Cell Carcinoma from the Randomized Phase III METEOR Trial

Candidate: **Tutor:**

Dr. Alessia Cimadamore Prof. Dr. Rodolfo Montironi

Anno Accademico 2020-2021

Summary

Abstract

Purpose: Anti-angiogenic VEGF-receptor (VEGFR) inhibitors are approved for metastatic renal cell carcinoma (RCC) and their efficacy is higher in high angiogenic tumors. As cabozantinib inhibits multiple tyrosine kinase receptors, including VEGFR, we tested whether markers of angiogenesis, including microvascular density (MVD) and mast cell density (MCD), could predict benefit from cabozantinib versus everolimus, using RCC samples from the METEOR (NCT01865747) trial.

Experimental design: MVD and MCD were studied in 430 patients (cabozantinib = 216, everolimus = 214) by double immunohistochemistry for CD31 (vascular marker) and tryptase (mast cell marker) coupled with automated image analysis. Results from evaluable cases (MVD = 360, MCD =325) were correlated with progression-free survival (PFS), overall survival (OS), overall response rate (ORR) and disease control rate (DCR).

Results: MVD was positively correlated with MCD. In the whole cohort, high MVD was associated with longer PFS and high MCD was associated with longer PFS and OS. Cabozantinib was associated with improved PFS, OS, ORR and DCR compared to everolimus, irrespective of MVD levels. Cabozantinib was also associated with improved ORR and DCR compared to everolimus, irrespective of MCD levels. For PFS and OS, the treatment effect for cabozantinib versus everolimus tended to be greater in tumors with low MCD.

Conclusions: High MVD and high MCD are associated with improved outcome in metastatic RCC, but fail to predict benefit to cabozantinib versus everolimus. The high efficacy of

cabozantinib in tumors with low angiogenic markers suggests that its anti-tumor activity in RCC is not predominantly mediated by VEGFR inhibition.

Introduction

Renal cell carcinoma

Renal-cell carcinoma is the most common form of kidney cancer and represents 5% of all cancers in men and 3% in women with more than 330,000 cases diagnosed and more than 140,000 deaths attributed to it worldwide every year[1]. Although the 70% of all RCC cases are diagnosed with early-stage or locally advanced disease, approximately the 20–40% of patients progress toward metastatic disease following radical surgery.[2] In the last 70 years, from 1952 to 2020, the clinical spectrum of renal cell carcinomas (RCC) has expanded by the increased recognition of new entities and the refinements of existing categories.[3,4] The most recent World Health Organization (WHO) classification of renal neoplasms account for more than 50 entities and provisional entities.[5] New entities might be included in the upcoming WHO classification.

Histopathological classification of RCC distinguish three most frequent subtypes: clear cell RCC, that accounts for the 70-75% of all RCC, papillary RCC (10-15%), and chromophobe RCC (5%).[5] However, besides an increasing understanding of the tumor histologies and biological behaviour, only few tumor entities have a specific treatment and ongoing clinical trial are still adopting the old classification of clear cells RCC (ccRCC) and non-clear cells RCC (nccRCC) as selection criteria.[6] Remarkable increase of knowledge about the genetic alterations of RCC in the last decade has led to greater understanding of the molecular pathogenesis of renal cancer and to the identification of novel therapeutic agents that are effective against RCC cells that have specific genetic changes.[7,8]

Over the past 6 years, significant genomic and transcriptomic studies performed on RCC by the Cancer Genome Atlas (TCGA) and also by individual laboratories presented a comprehensive molecular description of individual RCC pathogenic alterations.[9–11] Such molecular findings pave the way for an integrated classification, based on histopathology aspects and molecular alterations in order to personalize the clinical management of RCC.[12,13]

Table 1. Renal cell tumors and new described entities grouped according to their cellular features/architectural pattern, anatomic location, associated diseases, and genetic alterations (Reproduced from Cimadamore et al. Transl Androl Urol. 2021 Mar;10(3):1506-1520. doi: 10.21037/tau-20-1150.)[14]

Cellular features and/or Architectural pattern	Anatomic location	Associated diseases	Genetic alterations
• Clear Cell RCC • Papillary RCC • Chromophobe RCC • RCC with (angio)leiomyomatous stroma • Clear cell Papillary RCC • Biphasic squamoid papillary RCC • Mucinous tubular spindle cell carcinoma • HOT/LOT • Eosinophilic solid and cystic RCC • Tubulocystic RCC • Thyroid like follicular RCC • Papillary renal neoplasm with reverse polarity	• Renal medullary carcinomas • Collecting duct carcinomas	• Acquired cystic disease–associated RCC • RCC in neuroblastoma survivors	• TCEB1 RCC • MiT family translocation RCC • FH deficient RCC • ALK Rearrangement-Associated RCC • SDH- Deficient Neoplasia

A growing understanding of the underlying molecular biology of clear-cell RCC identified a central role of the von Hippel-Lindau (VHL) gene.[15] VHL signaling with its hypoxia-inducible

transcription factors (HIF1α, HIF2α) has notoriously being considered the main critical pathway for carcinogenesis in RCC, especially for the clear cell (ccRCC) histology. VHL inactivation occurs in over 70-80% of sporadic RCC, thorugh a gene mutation or less commonly through promoter methylation with consequent loss of function of the tumor suppressor protein (pVHL) codified by the VHL gene.[16] The main function of the pVHL is to determine the degradation of specific proteins by the attachment of polyubiquitin tails. [17]These tails serve as signals for such proteins to be destructed by the proteasome. The members of the HIF α family (HIF-1α, HIF-2α, and HIF-3α) are some of the proteins targeted by pVHL and its complex.[18] In tumor cells with loss of VHL function, or when oxygen is limiting, HIF proteins escapes degradation and forms dimers with the HIF-1β isoform. This so-formed complex is imported into the nucleus where is able to bind the DNA at the hypoxia response elements. This determines the transcription of multiple genes, such as vascular endothelial growth factor (VEGF), platelet-derived growth factor B (PDGFB), and transforming growth factor (TGF) α. The reintroduction of functional VHL protein in tumor cells have demonstrated to restore their control on the transcription of hypoxia-inducible genes.[19] Several therapeutics targeting this signaling pathway have been developed, respectively directed towards the tyrosine kinase (TK) domain of VEGF receptor (cabozantinib, axitinib, pazopanib, lenvatinib), or dual inhibitors towards VEGF and PDGF receptors (sunitinib, sorafenib), as well as a monoclonal antibody anti-VEGF (bevacizumab) and two PI3K/AKT/mTOR inhibitors (everolimus, temsirolimus)[20]. These drugs -in other words metabolic agents- have significantly improved patient survival outcomes. Currently, new small molecules that inhibit the linkage between HIF-2α and HIF-1β are under clinical investigation, especially

PT2399, a selective HIF-2 antagonist, based on the preclinical evidence that PT2399 affects cell replication and growth of both ccRCC cell lines and xenografts models.[21]

Papillary RCCs represents a heterogeneous disease, historically divided in:

• type 1 RCCs, more frequently associated to MET or epidermal growth factor receptor (EGFR) mutations

• type 2 RCCs often unique tumours with an aggressive phenotype that are associated with SETD2 mutations, CDKN2A mutations or TFE3 fusions[10].

On the other hand, Chromophobe RCCs display more frequent chromosome loss but fewer somatic mutations. The most frequently mutated gene is tumour suppressor protein 53 (TP53) (32%), and the most frequent oncogenic pathways involved in such tumours are mammalian target of rapamycin (mTOR) pathways (23%), including alterations of phosphatase and tensin homologue (PTEN).[22]

The prognostic factors validated by the International Society of Urological Pathology (ISUP) consensus and the WHO 2016 classification of RCC to be reported in routine practice are: the tumour histological subtype; the ISUP nucleolar grade (instead of the previous Fuhrman grade) that is only applicable to ccRCC and papillary RCC; a sarcomatoid and/or rhabdoid differentiation that defines a grade 4 tumour; the presence of necrosis; the presence of microscopic vascular invasion; the pathological tumour, node and metastasis (pTNM) staging and description of the non-neoplastic renal tissue.

Risk assessment models

The natural clinical course varies in RCC, which has led to the development of different prognostic models for the assessment of the patient's individual risk. In the metastatic setting the most used model are the Memorial Sloan Kettering Cancer Center (MSKCC) system and the subsequent refinements International Metastatic RCC Database Consortium (IMDC) score. Six factors are evaluated:

- Karnofsky performance status (PS) < 80%;
- Haemoglobin level below the lower limit of normal;
- Time from diagnosis to treatment < 1 year;
- corrected calcium above the upper limit of normal;
- platelets greater than the upper limit of normal
- neutrophils greater than the upper limit of normal.

The model holds its predictive value even in second and further lines of therapy and in non-clear histology tumors.

Current therapy guidelines for RCC

First-line standard-of-care treatments for patients with advanced renal cell carcinoma includes three VEGF-targeted agents that have demonstrated efficacy in pivotal phase III trials, mostly focused on good and intermediate patients: bevacizumab (combined with IFN), sunitinib and pazopanib. Second-line standard-of-care treatments include the VEGFR tyrosine-kinase inhibitors axitinib and sorafenib, the mTOR inhibitor everolimus, and the PD-1 checkpoint inhibitor nivolumab.[23,24] Few treatments have shown a survival benefit, and none have shown an

improvement in all three efficacy endpoints of progression-free survival, objective response, and overall survival, compared with standard-of-care treatment in a randomised phase 3 trial in previously treated patients with renal cell carcinoma

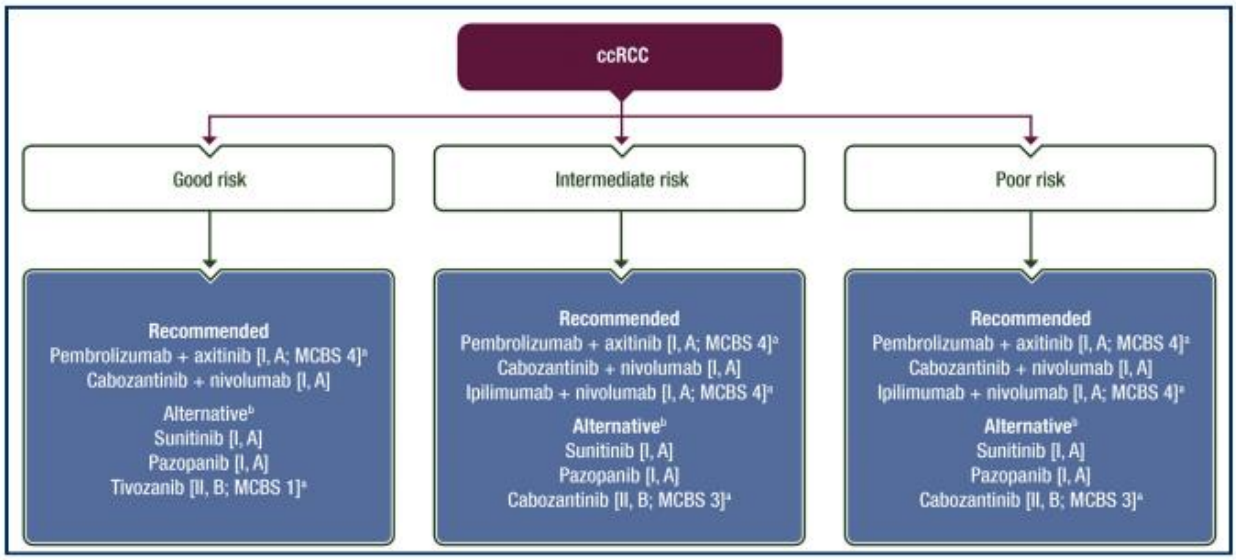

Vascular endothelial growth factor receptors (VEGFR)-tyrosine kinase inhibitors (TKIs) are approved treatments for patients with metastatic clear cell renal cell carcinoma (mccRCC), either as monotherapy or in combination with anti-PD-1 agents.[25–28]

There is both pre-clinical and clinical evidence that in ccRCC, the anti-tumor activity of VEGFR-TKIs is largely mediated by their anti-angiogenic effect[29–31]. Of note, recent data indicate that ccRCC tumors with high levels of vascularization respond better to these anti-angiogenic agents.[32]

Indeed, in mccRCC patients treated with the VEGFR-TKI sunitinib as part of the IMmotion 150 and IMmotion 151 trials, high expression of a 6-gene angiogenesis signature, including *PECAM1* (coding for CD31) was associated with improved ORR and PFS[33,34]. As expected, levels of the angiogenesis gene signature levels were strongly associated with levels of microvessel

density (MVD), assessed by CD31 immunohistochemistry, which is a well-established biomarker of angiogenesis[33]. More recently, results from IMmotion 150/151 trials were independently confirmed by analysis of the JAVELIN Renal 101 trial[35].

Cabozantinib is a multitarget TKI active against VEGFR, Met and Axl, among others. Its efficacy in treating mccRCC patients who progressed after previous VEGFR-TKI treatment[36] was tested in the METEOR (NCT01865747) trial, a randomised, open-label, phase 3, study with patients enrolled at 173 hospital and outpatient clinics in 26 countries. Inclusion criteria of METEOR trial were as follows:

- Documented histological or cytological diagnosis of renal cell cancer with a clear-cell component.
- Measurable disease as determined by the investigator.
- Must have received at least one VEGFR-targeting TKI (eg, sorafenib, sunitinib, axitinib, pazopanib or tivozanib).

Patients with previous mTOR inhibitor therapy, including everolimus, were not eligible for the study nor were patients with uncontrolled hypertension or clinically significant cardiovascular, gastrointestinal, wound healing, or infectious comorbidities. The aim of METEOR trial was to compare the efficacy and safety of cabozantinib versus the mTOR inhibitor everolimus in patients with advanced RCC who progressed after previous VEGFR TKI treatment. Progression-free survival in the first 375 randomised patients, the primary endpoint, was significantly improved with cabozantinib compared with everolimus treatment with a median progression-free survival of

7,4 months (95% CI 5,6–9,1) versus 3,8 months (3,7–5,4; HR 0,58, 95% CI 0,45–0,75; p<0,001) as assessed by an independent radiology review committee. [36]

In addition, cabozantinib has been shown to be more effective than sunitinib in the first-line setting[37]. More recently, the combination of cabozantinib plus the anti-PD-1 antibody nivolumab was also shown to be a valuable frontline treatment for patients with mccRCC[38].

Currently, it remains unclear whether cabozantinib superiority over earlier VEGFR-TKIs (i.e. sunitinib) is due to the inhibition of additional tyrosine kinase receptors (RTKs) (e.g. Met and Axl) or to a more potent inhibition of VEGFR2[39,40]. Understanding whether, similar to sunitinib, cabozantinib is more effective in patients with high-angiogenic tumors would not only shed important light on the role of VEGFR-inhibition in mediating the anti-tumor activity of cabozantinib in mccRCC, but could also lead to the identification of biomarkers of response to this agent, alone or in combination with other drugs.

PD-L1 expression and the immune environment in renal cell carcinoma

In the metastatic setting, the immunohistochemical expression of programmed death ligand 1 (PD-L1) is presently under the spotlight, although the results available so far are still controversial. In 2016, a systematic review and meta-analysis of 6 studies and 1323 cases clearly demonstrated a negative prognostic role of elevated level of PD-L1 tumour expression in RCC[41], although discrepancies between PD-L1 expression between the primary tumour and the metastases have been reported. A possible predictive value of PD-L1 expression remains controversial, although

recently, PD-L1 tumour expression was shown to be able to identify patients benefiting from a combination of two immune-checkpoint inhibitors.[42]

In the first trial, CheckMate 025[24], PDL1 status was assessed on tumor cells using Dako antibody anti-PD-L1. Membrane expression was assessed at a central laboratory with two cut-off: ≥1% vs. <1% and ≥5% vs. <5%. 24% and 11% of patients with a quantifiable PD-L1 expression had 1% or greater and 5% or greater PD-L1 expression, respectively. The benefit in OS observed with nivolumab was irrespective of PD-L1 expression. Similar conclusions were observed also among patients with 5% or greater PD-L1 expression, as compared with patients with less than 5% PD-L1 expression. In Checkmate 214[43], PD-L1 status was assessed by a central laboratory with the antibody clone 28-8 (Dako PD-L1) (Cut-off used: ≥1% vs. <1%). In this study 214/776 (27,5%) patients had 1% or greater PD-L1 expression. Patients with PD-L1 expression ≥1% showed higher ORR and PFS in the nivolumab plus ipilimumab arm compared to sunitinib; whereas, patients with favorable category of risk (which showed lower PD-L1 expression) showed a longer PFS and a higher ORR with sunitinib. A similar trend was observed among patients with 5% or greater PD-L1 expression, as compared with patients with less than 5% PD-L1 expression.

A different assay was applied in Keynote 426[44] and Keynote 427[45,46]. PDL1 status was assessed at a central laboratory according to the combined positive score (CPS), calculated as the number of PD-L1–positive cells (tumor cells, lymphocytes, and macrophages) divided by the total number of tumor cells, multiplied by 100 (antibody used: anti-PD-L1, 22C3 pharmDx assay, Agilent Technologies). In Keynote 426, 60.5% had a CPS of 1 or more. The benefit of pembrolizumab plus axitinib was observed in both PD-L1 expression subgroups. In Keynote 427 42% have a CPS

≥1 in cohort A (ccRCC) and 62% in cohort B (nccRCC). No data regarding association with PD-L1 status and outcome are available at this time.

In both trial IMmotion150[47] and IMmotion151[48] the investigators analyzed PD-L1 expression on tumor-infiltrating immune cells (IC) with the antibody SP142 (Ventana). Fifty-four% and 40% of patients had PD-L1 positive expression (≥1%) in IMmotion 150 – IMmotion151, respectively. In the phase II trial, patient with PD-L1+ tumor showed a longer PFS (14.7 months) and higher ORR (46%) in the atezolizumab plus bevacizumab arm compared to sunitinib. In the subsequent phase III trial, the PD-L1 positive population had a median PFS was 11,2 months in the atezolizumab plus bevacizumab group versus 7,7 months in the sunitinib group (HR: 0.74; p=0,0217). Of note, the PFS HR in patients with sarcomatoid histology was 0,46 in the PD-L1 IC positive population and 0,56 in the Intention-to-treat (ITT) population. Moreover, a gradient of increasing benefit with increasing levels of PD-L1 tumor-infiltrating IC expression was showed (PD-L1 expression on tumor infiltrating IC of 10% or greater: HR 0,56).

In the Atezo+Bev trial (NCT02724878)[49], PD-L1 double IHC staining was performed using a validated antibody against PD-L1 (405.9A11) (commercially available through Cell Signaling Technology). A panel of antibodies against immune cells (anti-CD45 and anti-CD163) was applied to distinguish tumor cells from immune cell infiltrate. Percentage of PD-L1 positive tumor cells (≥1% vs. <1%.) was assessed by two blinded genitourinary pathologists. 42% of tumors were PD-L1 positive and their ORR was higher (60%) compared to 19% in PD-L1 negative (p=0.01).

PD-L1 expression on tumor-infiltrating Immune cells (IC) was tested as biomarker in JAVELIN Renal 101[50]. IC status was assessed by a central laboratory with the use of the Ventana PD-L1 (SP263) assay (PD-L1–positive tumors if ≥1% of immune cells staining positive within the tumor

area of the tested tissue sample). 560 patients (63.2%) had a PD-L1 positive tumor. Among the patients with PD-L1-positive tumors, median PFS was significantly longer (13.8 months) with avelumab plus axitinib, compared with sunitinib (7.2 months) (HR 0.61; P<0.001); ORR was 55.2% in the combination arm vs. 25.5% with sunitinib.

Using biomarkers of a specific patient to predict the clinical response and provide a personalized therapeutic strategy would be the ideal approach in the clinical scenario. Currently, no predictive biomarkers are validated for use in RCC. The role of PD-L1 as a predictive biomarker is not clear and it is not comparable among these clinical studies. There are many reasons why this biomarker seems defective in kidney compared to lung, melanoma and bladder cancers. First, the nature of PD-L1 expression is dynamic, it changes between primary and metastatic tumors as well as the density of CD8+ T cells, supporting the need to evaluate distant sites for predictive biomarkers when treating metastatic disease.[51,52]

Second, the heterogeneity of expression in the same tumor slide and in the entire tumor impair the pathologist's evaluation of the staining.[53] Third, a lack of consensus methodologies on biomarker assessment. In many of the clinical trial, the PD-L1 status was assessed using different PD-L1 antibodies, different platforms and different methods of estimation.

Figure 1. Illustrations of PD-L1 IHC assays applied in checkpoint inhibitors trials in renal cell carcinoma. A: PD-L1 expression on tumor cells (TC); B: PD-L1 expression on tumor-infiltrating immune cells (IC); C: Combined Positive Score (CPS): number of PD-L1–positive cells (tumor cells, lymphocytes, and macrophages) divided by the total number of tumor cells, multiplied by 100.

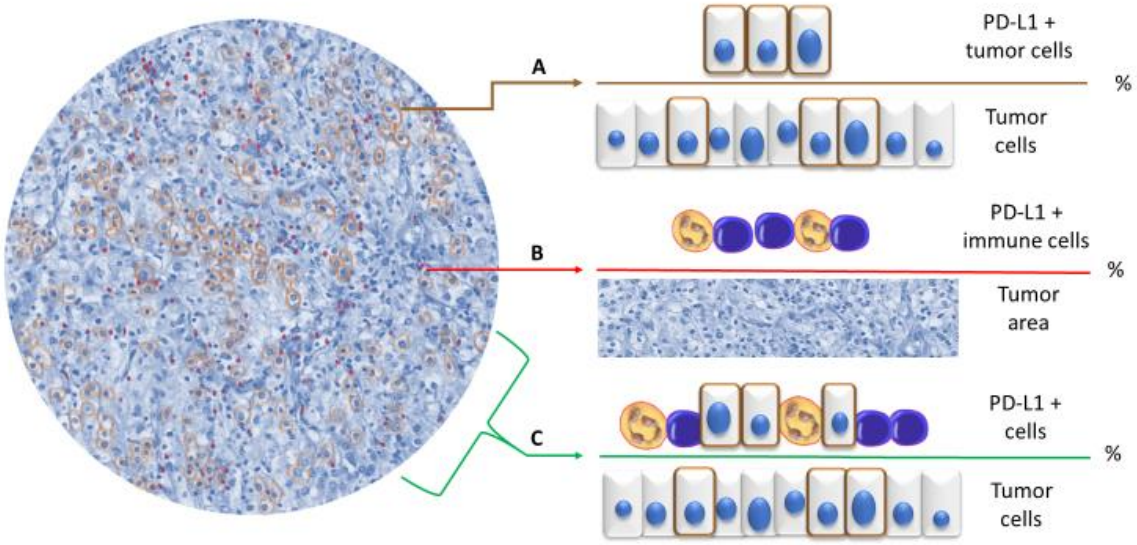

Cross-trial comparisons are limited by patient populations and study design. Moreover, the endpoints of all these studies on immunotherapy are based exclusively on RECISTv1.1 criteria. According to these criteria, patients with a new small lesion developed during treatment or with a tumor mass enlargement would be classified as early progressors instead of atypical responders' patients, applying immune-related response criteria (irRECIST). Re-evaluation of biomarkers of response to immunotherapy according to irRECIST criteria has been performed on CheckMate010, a phase 2 clinical trial evaluating nivolumab in monotherapy in 168 pretreated patients.[54,55] In this study, the median irPFSs were significantly longer than the median PFSs. Also, TC PD-L1 IHC expression was significantly associated with the median irPFS (15.4 months in PD-L1 positive group compared to 4.3 months in the PDL1< 1% group) and with irORR (47,4% vs. 19,3%) whereas there was no association with the standard PFS and ORR. The application of

traditional criteria to assess response in patients treated with immunotherapy might impair the discovery of potential predictive biomarkers.

Regarding the prognostic value of PD-L1, a meta-analysis of six published studies revealed that a higher level of PD-L1 expression increased the risk of death by representing, therefore, a negative prognostic factor.[41,56,57] The accurate analysis of the randomized clinical trials METEOR (NCT01865747)[57] and CABOSUN (NCT01835158)[36,58,59] reveals that higher PD-L1 expression correlate with a worse clinical outcome in mRCC treated with cabozantinib, everolimus (METEOR), or sunitinib (CABOSUN), but is not predictive of response to cabozantinib therapy. Previous treatments with VEGF-blockade can trigger anti-immune response by increasing the tumor infiltrating T cells.[60,61] Treatment with sunitinib have been associated with a reversible inhibition of specific lymphocyte subsets (CD3 and CD 4 T cells), and a decrease of regulatory T cells.[62,63] In the phase 3 IMmotion 151 the improvement in PFS in patients with PD-L1 positive tumors in the combination arm (anti-VEGF + anti-PDL1) was better in crossover patients than with the monotherapies in the same patients as front-line treatment. Indeed, in front-line setting, patients with T-effector–high and myeloid inflammatory–high signature experienced a reduced atezolizumab monotherapy activity thus suggesting a potential mechanism of immune escape, which may be overcome by the combination with bevacizumab.[64] The current use of combination of targeted therapy with immunotherapy makes the development of a biomarker more difficult.

The intricate interplay of inflammatory mediators and signaling pathways in a complex microenvironment is crucial for RCC development and response to therapy. It has been shown that PD-L1 expression is regulated by HIF in ccRCC.[47] The cellular type of inflammatory infiltrate, including T cells, neutrophils, dendritic cells, natural killer cells, and macrophages[65], the

intratumoral or peripheral location of the infiltrate, the density of microvessels and lymphatic vessels[33], the activation or exhaustion of inflammatory cells are potential characteristics that are being explored. Combined panels of biomarkers could be a potential solution to overcome the inconsistent value of PD-L1 expression as predictive biomarker. Pignon et al. found that the subset of patients with positive PD-L1 expression on TC and high percentages of CD8 expressing PD1 but not TIM-3 and LAG-3 exhibited the longest median irPFS (15.4 months) and the highest irORR (54,5%). As expected, the response to immunotherapy does not depends only on PD-L1 expression on tumor cells but on the type of tumor associated infiltrate and its level of exhaustion. Constant antigenic stimulation of CD8 T cells results in T cell exhaustion as demonstrated during chronic viral infections and cancers.[66,67] Exhausted CD8 T cells typically express inhibitory receptors, most notably PD-1. These mechanisms are at the basis of the development of PD-1–directed immunotherapy aiming to restore T-cell function.[68–70] Recent studies demonstrated that only a specific subgroup of T cells is responsive to the anti-PD1 therapy, hence their presence is critical for the effectiveness of PD-1 therapy. Only the subgroup with stem cell-like properties, identified by the expression of PD-1 and T cell factor 1 (TCF1), displays the proliferative burst seen after PD-1 immunotherapy and then differentiates to give rise to the more terminally differentiated/exhausted CD8 T cells.[71–73] This subgroup - terminally differentiated T cells - do not proliferate in response to re-stimulation and express high levels of checkpoint molecules. Jansen et al. hypothesized that the failure of the T cell response in tumors "is not caused by accumulation of checkpoint expressing exhausted CD8 T cells or overexpression of PD-L1 in the tumor, but by the failure of stem-like CD8 T cells to be sufficiently stimulated by an antigen-

presenting-cell niche to continuously produce terminally differentiated CD8 T cells in the tumor".[74]

PD-1 is also expressed on B cells, regulatory T cells, T follicular helper cells, NK cells, and myeloid cells. The mechanisms of PD-1 expression in myeloid cells and its role is still unknown but myeloid cell–specific PD-1 ablation seems to be is the key driver of antitumor immunity. Myeloid-specific PD-1 ablation more successfully decreased tumor growth compared with T cell–specific PD-1 ablation.[75]

Moreover, efficacy of PDL1 inhibitors could be impaired by administration of antibiotic therapy, a factor not evaluated by the cited trials. As showed by Routy et al. primary resistance to immune-checkpoint inhibitors can be associated to an abnormal gut microbiome composition. They demonstrated that fecal microbiota transplantation (FMT) from ICI responders' patients into germ-free or antibiotic-treated mice restored the therapeutic effect of PD-1 inhibitor, while FMT from nonresponding patients had no impact in terms of response.[76,77]

Angiogenic signature in Renal Cell Carcinoma

Several prognostic and predictive marker signatures have been described for specific systemic treatments in mRCC.[78] In the JAVELIN Renal 101 trial (NCT02684006), a 26-gene immunomodulatory gene signature predicted PFS in those treated with avelumab plus axitinib, while an angiogenesis gene signature was associated with PFS for sunitinib. Mutational profiles and histocompatibility leukocyte antigen (HLA) types were also associated with PFS, while PD-L1 expression and tumour mutational burden were not.[35] In IMmotion151 (NCT02420821), a T

effector/IFN-γ-high or angiogenesis-low gene expression signature predicted improved PFS for atezolizumab plus bevacizumab compared to sunitinib. The angiogenesis-high gene expression signature correlated with longer PFS in patients treated with sunitinib.[79] In CheckMate 214 (NCT02231749), a higher angiogenesis gene signature score was associated with better overall response rates and PFS for sunitinib, while a lower angiogenesis score was associated with higher ORR in those treated with nivolumab plus ipilimumab. Progression-free survival ≥ 18 months was more often seen in patients with higher expression of Hallmark inflammatory response and Hallmark epithelial mesenchymal transition gene sets.[80]

Microvasculature in solid tumors can be evaluated both qualitatively and quantitatively. Quantitative aspects of the angiogenesis research generally include intratumoral microvascular density (MVD), total microvascular area (TVA), or other less frequently used parameters such as vascular branching counts or some size- and shape-related variables.[81] Quantitative microvessel evaluation can be achieved either manually or in computer-assisted semi-automatic fashion.[82] These methods requires the use of specific markers to vascular endothelium and of immunohistochemical procedures to visualize microvessels. Some authors considered any stained CD31+ endothelial cell or CD31-positive cell cluster separated from other microvessel structures as a countable microvessel. Microvessel density was defined as the average count of microvessels from 10 random fields.[83] Other researchers used antibodies against CD34 to identify the microvessel endothelium. The counting methods included estimation of intratumoral MVD by one hot-spot, MVD by the mean value of three hot-spots, and the highest value of MVD in three hot-spots. However, these methods suffer from an high interobserver variability and poor

standardization and applicability in routine practice. On the other hand, software-assisted automatic methods are reproducible, but more time consuming and more expensive.

Role of mast cells in cancer

Increased accumulation of mast cells within tumor environments has been correlated with poor prognosis, increased metastasis and reduced survival in several types of human cancer, including melanoma[84], prostate[85], pancreatic adenocarcinoma [86], squamous cell carcinoma [87].

Tumor cells produce inflammatory mediators and pro-angiogenic factors, including stem cell factor (SCF). SCF is the ligand for CD117, also known as KIT receptor, a tyrosine kinase receptor highly expressed by mast cells[88]. Activation of SCF/Kit pathway is necessary for the maturation, migration and survival of mast cells[89], since they derive from hematopoietic precursors inside the bone marrow and complete their differentiation and maturation within vascularized tissues.[90] The surrounding environment of tumors, through SCF chemotaxis, promotes infiltration and maturation of mast cells, which release angiogenic mediators, proteases and growth factors that support tumor development.[91] It has been demonstrated that FGF-2 and VEGF derived from mast cells trigger an intense angiogenic response *in vivo*.[92] In agreement, accumulation of mast cells is usually found in the proximity of CD31+ cells and microvessels.[93]

Mast cells also release proteases within tumor environment. For example, tryptase activates latent metalloproteinases, contributes to extracellular matrix degradation, vascular tube formation and release of trapped angiogenic factors[94], promoting angiogenesis and metastasis. During tumor progression, mast cells also act on recruitment of neutrophils and eosinophils, activation of T and

B immune responses[95], and myeloid-derived suppressor cells, which accumulate in the tumor microenvironment and correlate with poor prognosis.[96]

Therefore, mast cells can exert pro-tumor effects by influencing the microenvironment or, directly, by conditioning the fate of tumor cells including drug resistance. They can promote tumor growth by inducing angiogenesis and promote tissue remodeling through the induction of changes in composition of the extracellular matrix.[97] Mast cells can also promote pro-inflammatory pathways that could result in the impairment of tumor progression.[98] The ability of mast cells to rapidly sense the environment could determine the resultant immune responses to tumors. By their ability to contribute to both innate and adaptive responses, mast cells can therefore modulate the outcome of major immune infiltrates present in tumors (i.e. TAM and lymphocytes). Therefore, we believe that targeting the survival/function of mast cells could influence cancer cells' behavior and therefore the outcome of clinical responses.

Infiltration of mast cells in the renal interstitium is associated with kidney diseases, such as glomerular diseases.[99] Moreover, mast cell counts in human kidney cortex were significantly increased in patients with chronic renal failure, and there was a significant relationship between serum creatinine and the mast cell granulation index.[100] Previously, mast cells were observed to highly infiltrate RCC tissues compared with non-neoplastic kidney tissues.[101] However, the relationship between mast cells and angiogenesis in RCC remains controversial. Tuna *et al.* observed a significant correlation between the number of mast cells and MVD in 71 RCC patients.[102] However, studies from Mohseni failed to demonstrate a positive correlation between the number of mast cells and MVD in RCC tumors using a smaller number of cases in their studies.[103] Using 125 RCC samples and 52 adjacent kidney tissue samples to assess mast cells and

endothelial cells, we found that there were more mast cells accumulated in RCC tissues than adjacent kidney tissues. More importantly, there was a significant correlation between MCD and MVD.

In literature, recruitment of mast cells resulted in increased RCC angiogenesis in both *in vitro* cell lines and *in vivo* mouse models. Mechanistic analyses revealed that RCC recruited mast cells by modulating PI3K→AKT→GSK3β→AM signaling. Higher expression of the PI3K→AKT→GSK3β→AM signaling pathway correlated with increased angiogenesis. Interruption of PI3K→AKT→GSK3β→AM signaling via specific inhibitors led to decreased recruitment of mast cells, and targeting this infiltrating mast cell-related signaling via an AKT-specific inhibitor suppressed RCC angiogenesis in xenograft mouse models.[104–107]

Recently, a paper published in Cancer Cell showed that melanoma and lung cancer patients who took antihistamines during immunotherapy treatment had significantly improved survival. The reason behind this evidence is the fact that histamine and histamine receptor H1 (HRH1) are frequently increased in the tumor microenvironment and induce T cell dysfunction. HRH1-activated macrophages polarize toward an M2-like immunosuppressive phenotype with increased expression of the immune checkpoint VISTA, rendering T cells dysfunctional. HRH1 knockout or antihistamine treatment reverted macrophage immunosuppression, revitalized T cell cytotoxic function, and restored immunotherapy response.[108]

Objectives

We tested the prognostic and predictive value of makers of angiogenesis in pre-treatment tumor tissues from patients who received either cabozantinib or everolimus within the METEOR trial. We decided to focus on protein markers analyzed by immunohistochemistry because, in contrast to RNA-based biomarkers, are very cost-effective and can be widely implemented in diagnostic laboratories throughout the world. Specifically, we measured MVD by assessing CD31 expression on endothelial cells in whole tissue sections. Moreover, we quantified mast cell infiltration as these immune cells are known to promote angiogenesis in human cancer, including RCC, both through VEGF-dependent and -independent pathways.

Materials and Methods

Study Design and Clinical Endpoints

Microvascular density (MVD) and Mast Cell density (MCD) were assessed on pretreatment tumor tissue samples (archival nephrectomy specimens n= 299 or metastases biopsy n= 31) of patients from the METEOR randomized phase III clinical trial. In the METEOR trial, cabozantinib was compared to everolimus in patients with mRCC who had progressed after previous VEGF TKI treatment[59]. Baseline demographics, clinical characteristics, and treatment outcomes, including overall response rate (ORR, including complete response and partial response), disease control rate (DCR, including complete response, partial response, and stable disease), PFS, and OS, were collected from the trial database. PFS and ORR (per RECIST 1.1) were determined by an independent radiology review committee assessment. PFS was defined as the time from randomization to radiographic progression or death from any cause and censored at date of last disease assessment; OS was calculated from randomization to date of death from any cause and censored at date of last follow up

This study was approved by the Institutional Review Board or ethics committee of the participating centers and was conducted in accordance with the Declaration of Helsinki and the Good Clinical Practice guidelines. All patients provided written-informed consent.

Immunohistochemistry staining

IHC staining were performed on formalin-fixed paraffin-embedded (FFPE) tissue sections collected by the study sponsors at enrolment. An in-house double IHC staining assay using anti-CD31 antibody (1:100, JC70A mouse monoclonal antibody, Dako) and anti-tryptase antibody (1:5000, AA1 mouse monoclonal antibody, Dako). Tumor sections were stained with a Bond III Autostainer (Leica Biosystems) using a Bond Polymer Refine Detection Kit (DS9800; Leica Biosystems) for the anti-CD31 stain and a Bond Polymer Refine Red Detection Kit (DS9390, Leica Biosystems) for the anti-tryptase stain. Antigen retrieval was performed with Bond Epitope Retrieval Solution 2 (EDTA, pH = 9.0) for 20 minutes before the anti-CD31 stain. Following the anti-CD31 staining, antibody stripping was performed with Bond Epitope Retrieval Solution 1 (Citrate, pH = 6.0) for 10 minutes prior to the anti-tryptase stain. All slides were counterstained with hematoxylin, dehydrated in graded ethanol and xylene, mounted, and coverslipped.

Met and PD-L1 protein expression data were available from previous studies[36,60]. Met protein levels were analyzed in immunohistochemistry with the SP44 antibody (Spring Biosciences, Pleasanton, CA,USA) in a centralized laboratory (LabCorp - Research Triangle Park, NC, USA).

MET expression was defined as high versus low, based on a cutoff of 50% or higher of tumour tissue stained with an intensity of 2+ or 3+ by immunohistochemistry.

PD-L1 expression was assessed by immunohistochemistry with an in-house double IHC staining assay, developed using an extensively validated antibody against PD-L1 [405. 9A11 mouse monoclonal antibody, 1:100,13 mg/mL, Dr. Freeman laboratory, Dana-Farber Cancer Institute, Boston, MA, and commercially available through Cell Signaling Technology (CST) and a cocktail

of antibodies recognizing IC consisting of anti-CD45 (1:500, D9M8I XP, rabbit monoclonal antibody, CST) with antiCD163 (1:5,000, EPR19518, rabbit monoclonal antibody, Abcam).

Scoring of IHC staining by image analysis

Immunostained slides were scanned at 200x magnification using Aperio ScanScope (Leica Microsystems) and quantified using Indica Lab HALO platform algorithms. In each slide, TC were identified using the HALO platform tissue classification module, and the number of PD-L1–positive TC was determined using the HALO platform multiplex-IHC v1.2 algorithm. CD45/CD163 staining was used to identify tumor-infiltrating IC. The HALO platform multiplex-IHC v1.2 algorithm was also utilized to determine the number of PD-L1–positive IC. Results of the image analysis were validated through visual inspection by pathologists with expertise in the evaluation of PD-L1 staining in RCC. Specifically, for each immunostained slide, pathologists confirmed that (1) the classifier correctly identified the TC and IC, and (2) the algorithm correctly identified the PD-L1–positive cells. Percentages of PD-L1–positive TC, PD-L1–positive IC, and combined TC/IC score (defined as [(number of PD-L1–positive TC þ number of PD-L1–positive IC)/(total number of TC) x100; ref. 28] were then calculated. For each tumor, positive TC PD-L1 expression was defined as 1% expression on TC. For PD-L1 positivity on IC and combined scores, two cutoffs (1% or 5%) were explored. For patients with multiple tissue samples analyzed, highest PD-L1 expression scores were used in subsequent analyses. To measure the total amount of tumor-infiltrating IC, we calculated immune cell density (ICD) scores defined as [(total number of IC/(Area occupied by tumor cells þ stromal area)] for each tumor tissue specimen. ICD scores

were then divided into tertile groups (low, intermediate, and high) using 33% and 66% as cutoffs from the joint distribution of ICD from the two trials.

Image Analysis for assessment of MVD and MCD

Immunostained slides were scanned at 20x magnification using an Aperio Versa (Leica Biosystems) and analyzed using Indica Lab HALO platform algorithms.

The first step to analyze the images was slide annotation. For each slide, tumor areas were manually annotated by research assistants (EW, MSI) and reviewed by pathologists (TD, AC). Areas of necrosis and of intervening stroma were excluded from the analysis. **Figure 2** shows the tumor area included within the light blue line, while the dotted line shows the excluded areas.

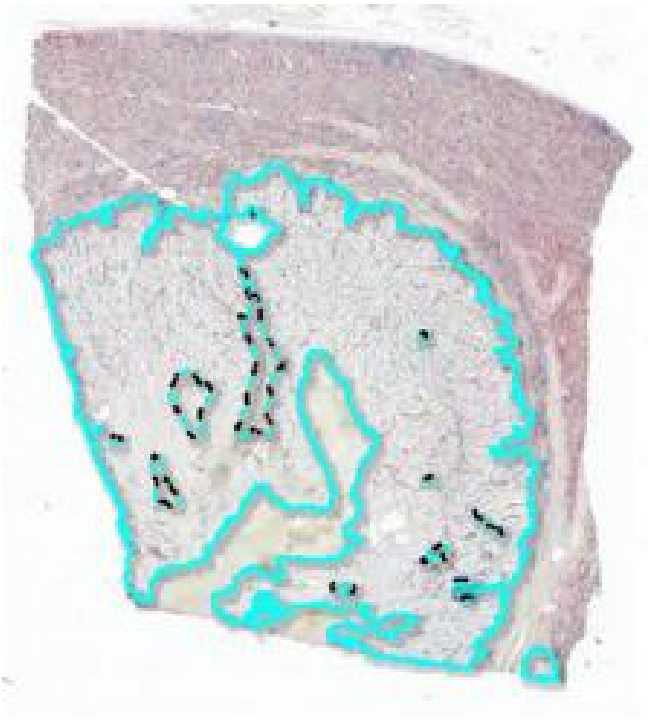

Background staining as well as macrophages positive for CD31 expression were excluded using the HALO platform tissue classification module. The tissue classifier module uses a machine learning algorithm to identify tissue types based on color, texture and contextual features. The pathologists in this case highlighted a few distinc tissue types (i.e. tumor, stroma, necrosis) and within seconds the software learned to categorize tissue.

The numbers of microvessels and mast cells were determined using the HALO platform colocalization v1.3 algorithm. For each immunostained slide, two pathologists (TD, AC) confirmed that i) the algorithms correctly identified the microvessels and the mast cells and ii) the classifier correctly excluded the macrophages stained by anti-CD31 antibody.

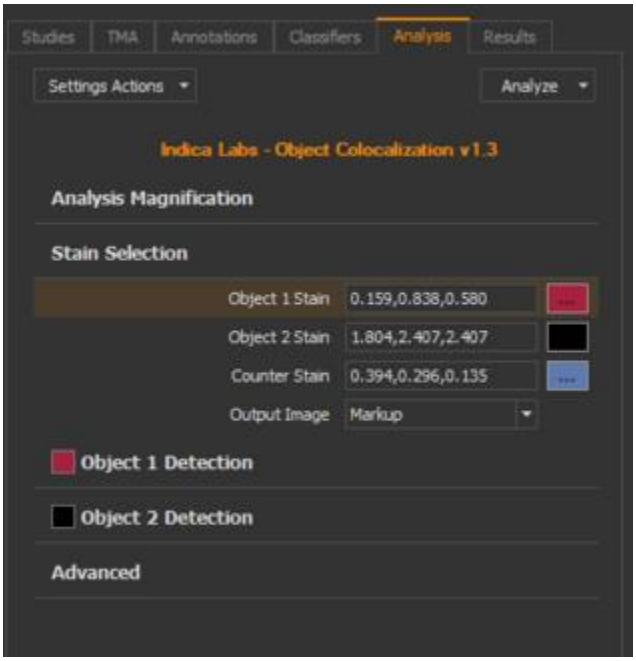

Figure 3. Tab of the HALO Software in which are showed the intensity setting thresholds for object 1 – red staining for mast cells, object 2 – dark brown staining for CD-31 vessels, and the counter staining (hematoxylin) for nuclei.

Both pathologists were blinded to the status of clinicopathologic information and information on clinical outcome. MVD and MCD were then calculated for each slide as number of objects identified (vessels and mast cells, respectively) in the tumor area. For patients with multiple tissue samples, the highest MVD and corresponding MCD were used for subsequent analyses.

Statistical analysis

To explore the association microvascular density and mast cell density with clinical outcomes, initially patients were grouped into low, medium and high levels based on using the tertile cut-points for each measure. Since low and medium tertile levels featured similar association with outcomes, therefore two groups were merged and each measure was dichotomized at the upper 33 percentile value for the 'high' group.

To evaluate the association of MVD and MCD by IMDC risk group, tumor grade, MET and PDL1 status Wilcoxon rank sum test was applied. To check association between MVD/MCD and MET and PDL1 status generalized linear models were considered adjusted for tumor grades.

Distributions of PFS and OS were estimated using Kaplan Meier methodology along with a 95% confidence interval (95%CI). Both Univariate and multivariable Cox proportional hazards models were conducted to estimate association with PFS and OS; Wald chi square test was provided. The multivariable models were adjusted for treatment, IMDC risk group, presence of bone metastases and number of previous VEGFR TKI treatment (1 or ≥2). Cochran-Armitage trend test was used to compare ORR and DCR among the ordered levels. Fisher's exact test was conducted to compare ORR and DCR for dichotomized markers.

To explore the predictive value of the MCD and MVD, we fit Cox regression models with the interaction term of treatment group and each biomarker and assessed hazard ratio for treatment comparison on PFS and OS by MCD and MVD levels (high and low), both unadjusted and adjusted interaction models were calculated. Test for interaction (p-interaction) was provided to assess whether treatment effects differed by biomarker groups. Unadjusted logistic regression model was conducted to assess treatment effects differed by biomarker groups for ORR and DCR.

Similar analyses were conducted for the combination of MCD and MVD and the combination of two biomarkers with MET status.

SAS version v9.4 (Cary, NC, USA) was used to carry out the above analysis. All statistical tests were two-sided.

Results

Patients characteristics and treatment

From August 2013 to November 2014, 658 patients were enrolled in the METEOR trial and randomly assigned (1:1) to receive either cabozantinib (n=330) or everolimus (n=328) as previously described [36]. Data cut-off was May 22, 2015 for PFS and response evaluation while for OS the data cutoff was December 31, 2015.

Patient demographic and clinical characteristics were similar in the subset of patients with available tissue specimens as compared with the overall trial population **(Table 2)**.

Table 2: Patient demographic and clinical characteristics

	N. of patients in MVD and MCD Cohort (N=360)		**Total (N=658)**	
	N	%	N	%
Gender				
Female	87	24	163	25
Male	273	76	494	75
Geographic region				
Europe	186	52	320	49
Nrth America	139	39	240	36

Other	35	10	98	15
Race				
White	288	80	532	81
Asian	18	5	47	7
Black	4	1	9	1
Other	26	7	32	5
Nt reported	24	7	37	6
Missing	-	-	1	0
ECOG performance status				
0	243	68	442	67
1	117	33	216	33
MSKCC risk factors				
0	169	47	300	46
1	155	43	273	41
2 or 3	36	10	85	13
IMDC risk group				
Favorable	74	21	128	19
Intermediate	241	67	424	64
Poor	45	13	106	16

Bone metastasis				
N	279	78	516	78
Yes	81	23	142	22
Liver metastasis				
N	255	71	467	71
Yes	105	29	191	29
Prior nephrectomy				
N	34	9	96	15
Yes	326	91	562	85
Prior VEGFR-target TKI Therapy				
1	260	72	464	71
2 or more	100	28	194	29

Biomarkers' assessment evaluation with image analysis

MVD and MCD density were studied in 430 patients (cabozantinib = 216, everolimus = 214) with tissue available tissue specimens. Evaluable data were obtained in 360 patients (cabozantinib = 175, everolimus = 185) for MVD. Among these 360 patients, 325 patients (cabozantinib = 159, everolimus = 166) had evaluable data for MCD **(Figure 4)**.

Figure 4: CONSORT Diagram

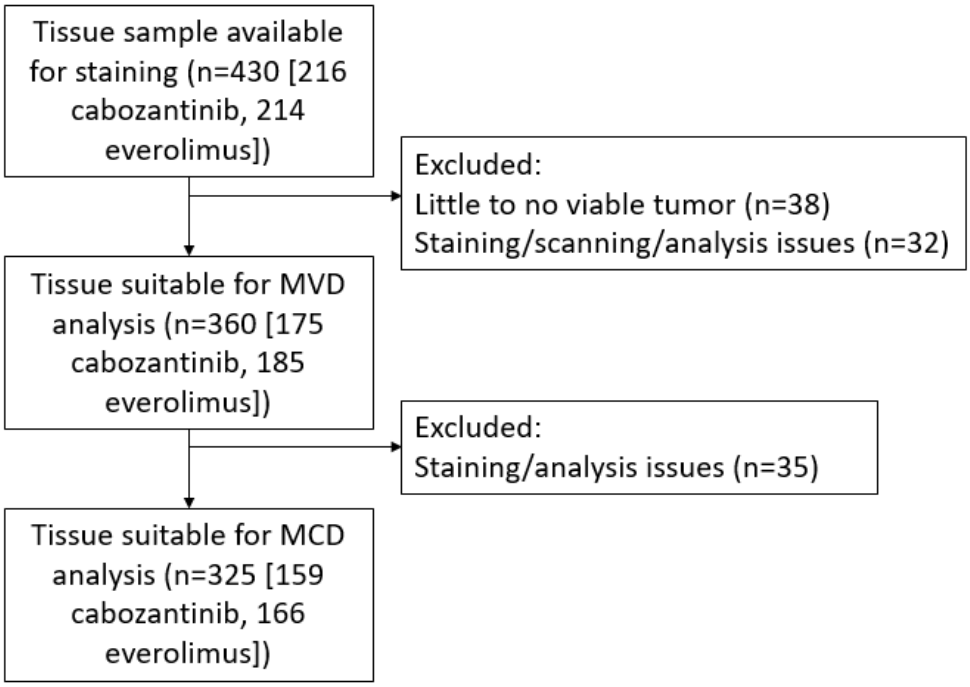

Median MVD and MCD were 147 MV/mm2 (range 8.8-750.4) and 7 MC/mm2 (range 0-72.8 MC/mm2), respectively.

Figure 5. Immunohistochemical slides stained with both triptase and CD-31 antibody before and after image analysis for mast cells (mast cells identified by red colour and square).

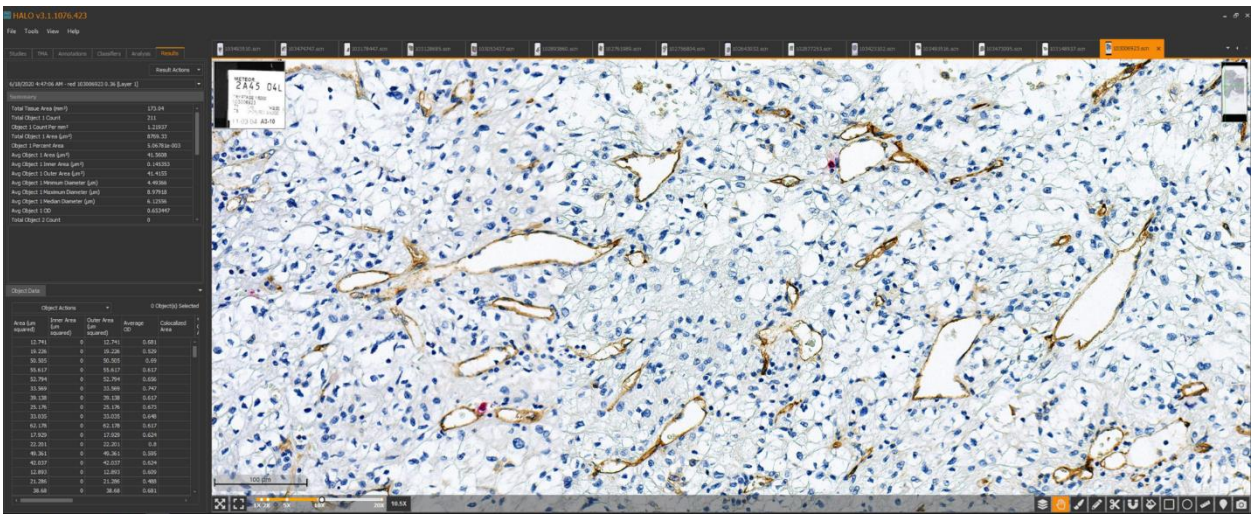

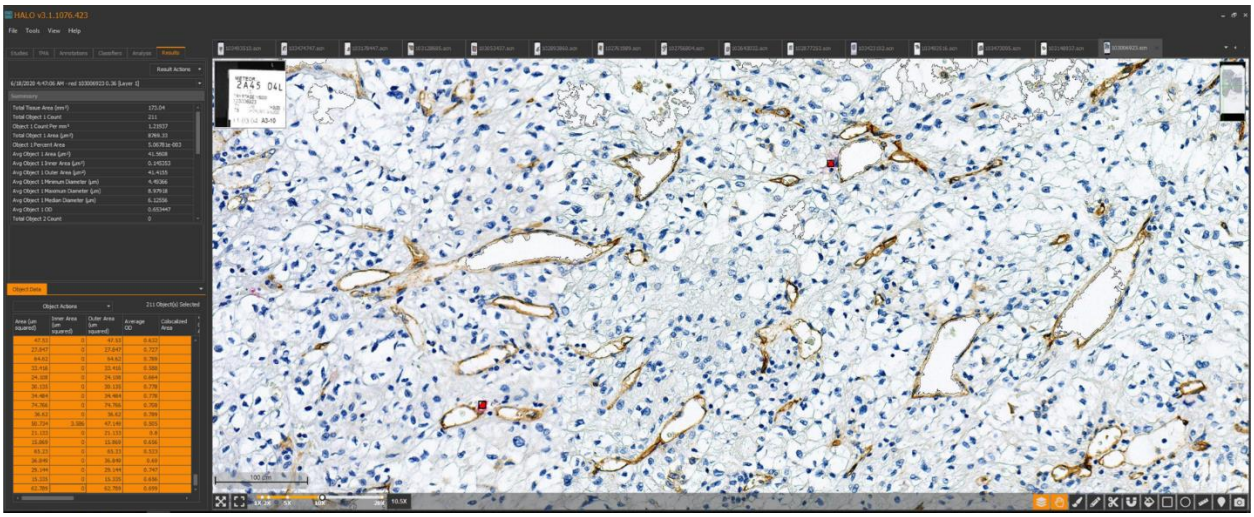

Figure 6. Immunohistochemical slides stained with both triptase and CD-31 antibody before and after image analysis for microvascular density (vessels identified by red colour and square).

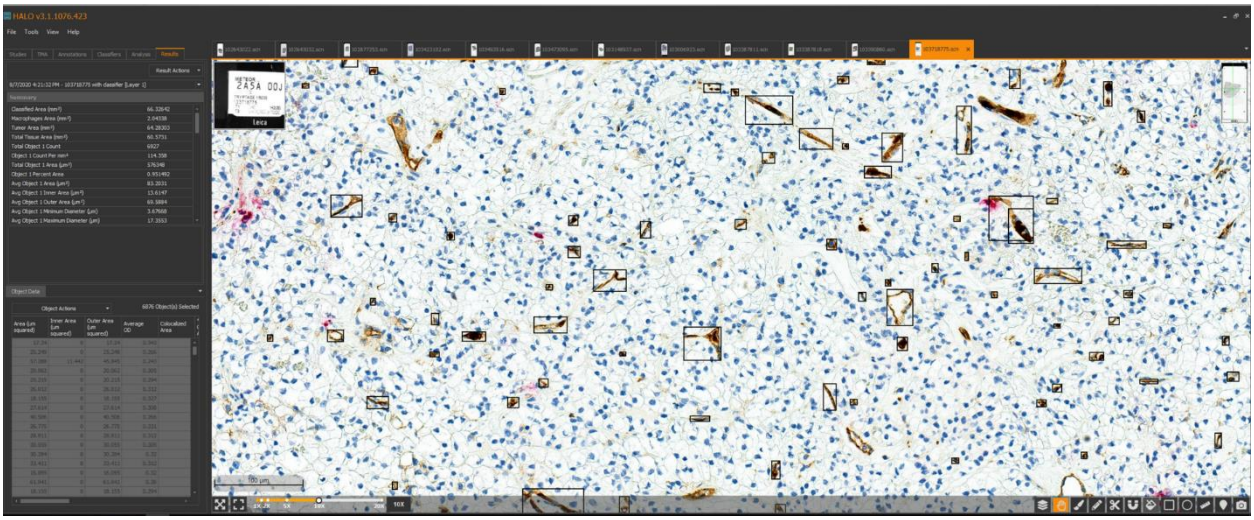

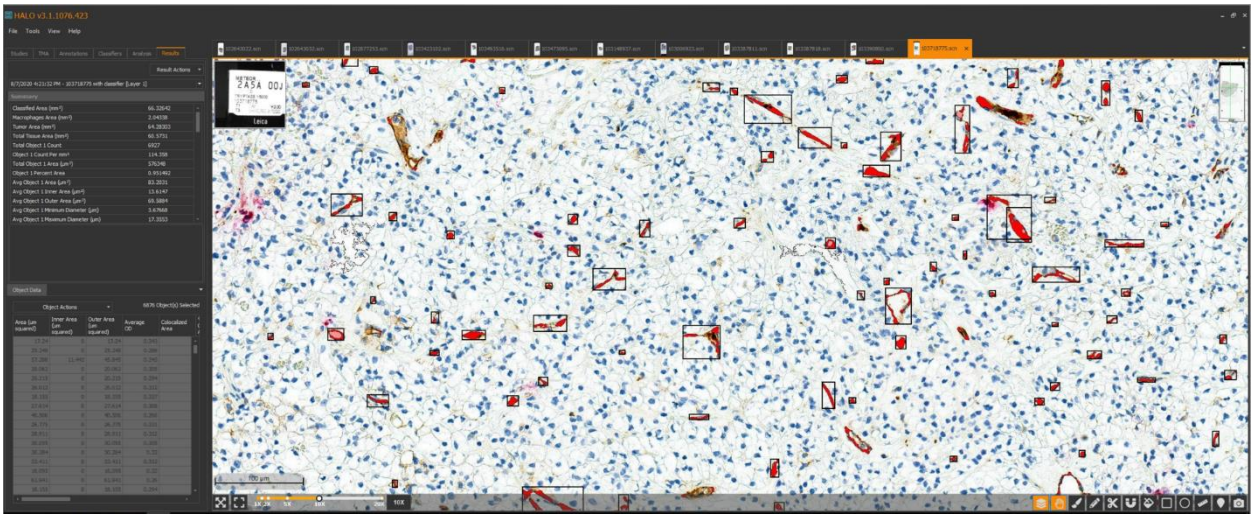

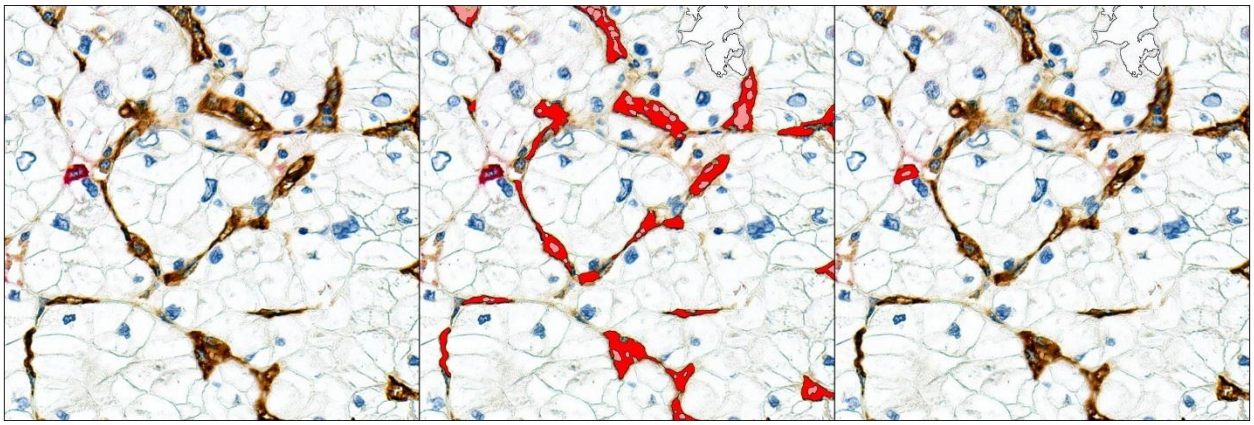

Representative image of ccRCC tissue double immunostained for CD31 (brown) and tryptase (red); b) markup image generated by the microvascular density algorithm; c) markup image generated by the mast cell density algorithm.

Association of microvascular density and mast cell density with clinicopathological features

In line with previous studies, we observed that MVD was positively correlated to MCD, with a Spearman correlation coefficient of 0.42 ($p<0.0001$) **(Figure 7)**.

Figure 7. Scatter Plot of the correlation between Microvascular Density and Mast Cell Density

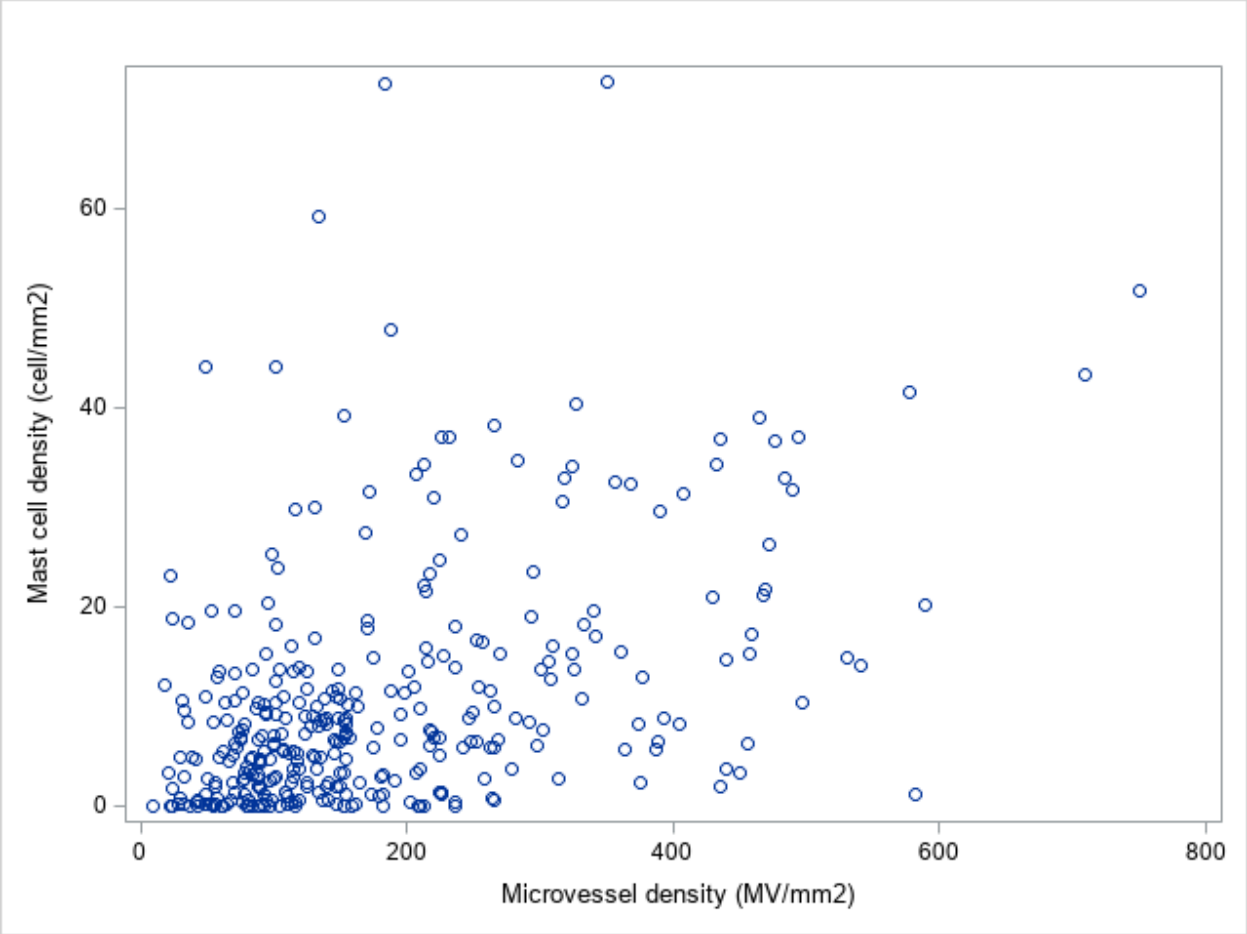

Both MVD and MCD were found to be negatively associated with tumor grade ($p< 0.0001$ for MVD and $p=0.04$ for MCD). Moreover, MCD levels were associated with IMDC risk groups at baseline, with higher levels observed in patients with favorable risk ($p=0.006$). A trend toward an

association between MVD levels and IMDC risk groups at baseline was observed (p=0.2). Finally, MVD levels were higher in tumors negative for PD-L1 expression and in tumors negative for Met expression **(Table 3)**.

Table 3. MVD and MCD by IMDC risk groups, Tumor Grades, MET and PDL1 status

		MVD			**MCD**	
	N	**Median (IQR)**	**p-value***	**N**	**Median (IQR)**	**p-value***
All pts	**360**			**325**		
Treatment Arms						
Cabo	175	148.5 (90.6-261.8)	0.3952	163	6.9 (2.3-13.8)	0.7911
Eve	185	135.6 (89.7-225.7)		177	7.0 (2.6-13.9)	
IMDC Risk Group						
Favorable	74	161.3 (98.4-279.1)	0.2194	69	9.8 (5.4-21.7)	0.0063
Intermediate	241	145.2 (88.6-226.2)		218	6.6 (2.4-13.5)	
Poor	45	133.1 (94.2-224.9)		38	7.5 (2.4-15.1)	
Tumor Grade	N=354			N=320		
2	99	217.3 (135.6-313.7)	<.0001	92	9.3 (3.7-18.2)	0.0445

3	171	139.6 (89.7-225.7)		154	7.5 (2.8-13.9)	
4	84	100.9 (75.6-157.8)		74	6.2 (2.4-9.1)	
Met	N=254			N=226		
Negative	200	152.4 (100.9-265.2)	<.0001 (<.0001**)	176	7.8 (3.3-14.0)	0.2394 (0.4688**)
Positive	54	93.5 (65.0-153.5)		50	7.0 (1.2-10.9)	
PDL1	N=270			N=242		
Negative	196	154.6 (94.8-271.0)	<.0001 (0.0052**)	177	8.3 (3.4-15.2)	0.0760 (0.8094**)
Positive	74	105.4 (76.0-161.1)		65	5.8 (2.5-10.5)	

*Wilcoxon rank sum test.
**Adjusted for tumor grades

Association of microvascular density with clinical outcomes

As previous studies have shown that MVD is associated with favorable prognosis in localized ccRCC[109], we investigated its association with clinical outcome in patients with metastatic ccRCC treated with targeted therapies. In this analysis, patients were initially divided into low, medium and high MVD groups using tertile cut points. There is no established cutoff for MVD and MCD. We have checked the optimal cutoff based on the Minimum P-value approach based on Wald test from Cox regression for PFS. The optimal cut points for both markers are close to the upper 33% percentile (208.2 for MVD and 11.3 for MCD) that we used in the analysis. The low and medium tertile groups featured similar association with outcomes **(Figure 8a-b)** and, therefore, the upper tertile cut-point was selected to categorize patients in MVD-high and MVD-low dichotomous groups.

Figure 8. Kaplan Meier Curves of PFS and OS by MVD tertile groups. a) PFS by MVD groups b) OS by MVD groups.

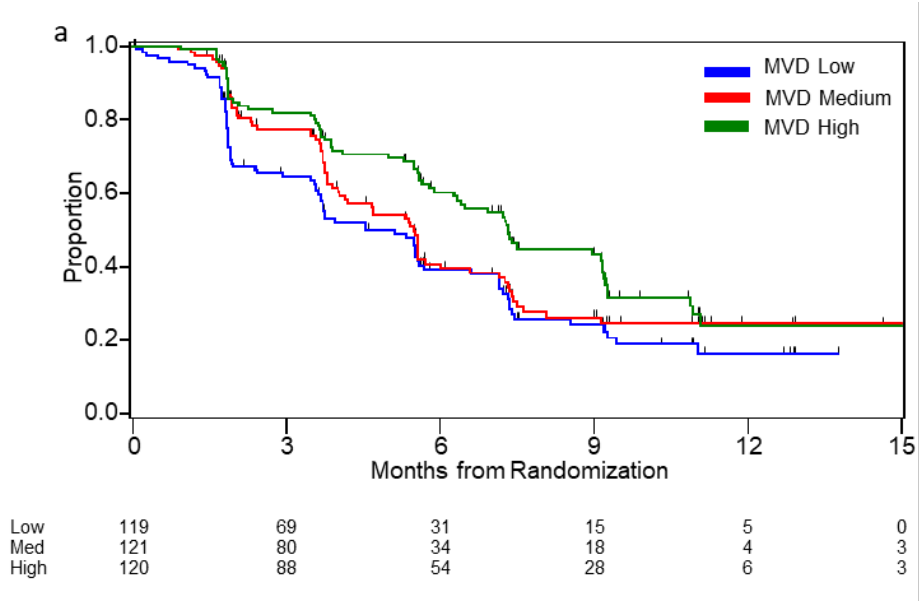

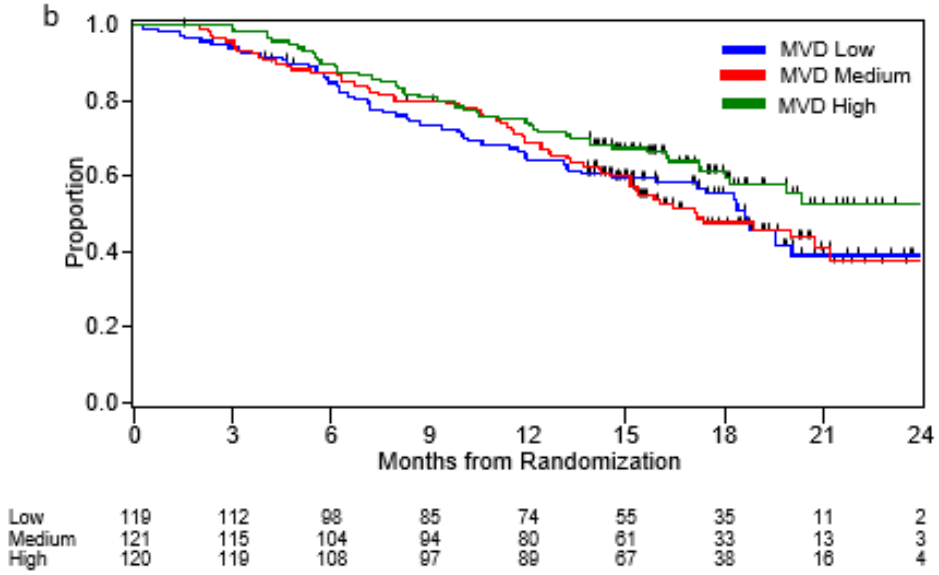

In the whole cohort, patients with high MVD had significantly longer median PFS compared with patients with low MVD (7.3 months vs. 5.4 months, HR 0.66, 95% CI 0.50-0.88), on univariate analysis **(Table 3, Figure 8a)**. On multivariate analysis, adjusted for treatment, IMDC risk group, presence of bone metastases and number of previous VEGFR TKI treatment (1 or ≥2), median PFS continued to be significantly longer in patients with high MVD compared with patients with low MVD (adjusted HR 0.69, 95% CI 0.52-0.93) **(Table 3)**. MVD was not associated with ORR, DCR **(Table 4)** or OS (**Table 3, Figure 8b)**.

Table 3. Association of MVD and MCD dichotomous groups with PFS and OS

		Univariate Analysis		Multivariable Analysis	
	N. of events/ N. of Patients	**Months, Median (95% CI)**	**Unadjusted* HR (95% CI)**	**Adjusted* HR (95% CI)**	**Adjusted* p-value**
Microvascular density					
OS					
Low (≤208.2 mm^2)	121/240	18.37 (15.87-20.01)	Ref.	Ref.	*0.1407*
High (>208.2 mm^2)	48/120	NR (18.04-NR)	0.72 (0.51-1.00)	0.78 (0.55-1.09)	
PFS					
Low (≤208.2 mm^2)	154/240	5.39 (3.94-5.55)	Ref.	Ref.	*0.0144*
High (>208.2 mm^2)	66/120	7.33 (6.28-9.17)	0.66 (0.50-0.88)	0.69 (0.52-0.93)	
Mast cell density					
OS					
Low (≤11.3 mm^2)	110/216	18.37 (15.87 - 19.55)	*Ref.*	*Ref.*	
High (>11.3 mm^2)	39/109	NR (20.37-NR)	0.66 (0.44- 0.92)	0.69 (0.48-0.99)	*0.0451*
PFS					
Low (≤11.3 mm^2)	142/216	5.49 (4.04-5.55)	*Ref.*	*Ref.*	
High (>11.3 mm^2)	54/109	7.46 (7.23-9.17)	0.64 (0.47-0.87)	0.66 (0.48-0.91)	*0.0112*

* Adjusted for IMDC risk group, presence of bone metastases and number of previous VEGFR TKI treatment (1 or ≥2)

Table 4. Association of MVD and MCD with ORR and DCR

MVD		
ORR	**N ORR/Total**	**ORR (%)**
Low	24/240	10%
High	12/120	10%
p-value*		0.99
DCR	**N DCR/Total**	**DCR (%)**
Low	171/240	71%
High	95/ 120	79%
p-value*		0.1267
MCD		
ORR	**N ORR/Total**	**ORR (%)**
Low	14/216	11%
High	9/109	8%
p-value*		0.5599
DCR	**N DCR/Total**	**DCR (%)**
Low	156/216	72%
High	87/109	80%
p-value*		0.1759

* Fisher exact test

Figure 8c-d. Kaplan Meier Curves of PFS and OS by MVD levels (dichotomous by upper 33% percentile). c) PFS by MVD groups d) OS by MVD groups

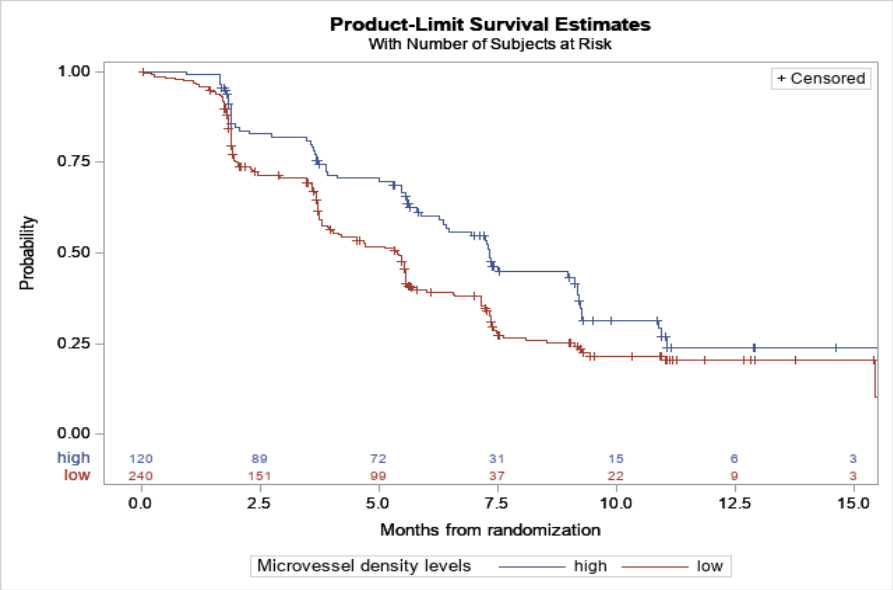

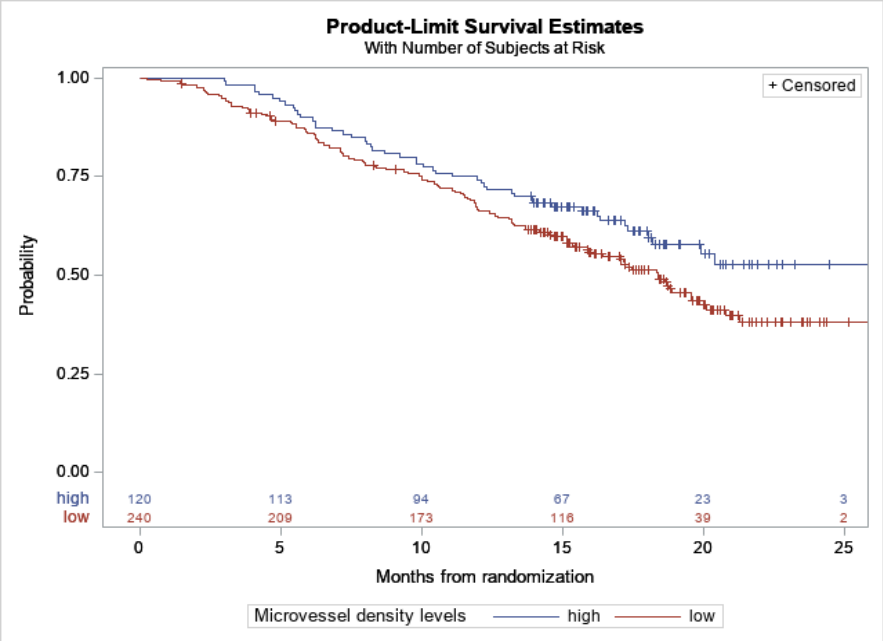

Since the mechanism of action of cabozantinib involves inhibition of angiogenesis by targeting tyrosine kinase receptors including VEGFRs, we hypothesized that patients with high MVD would receive greater benefit from cabozantinib compared to patient with low MVD. In contrast to our expectation, treatment with cabozantinib was associated with improved PFS, OS, ORR, and DCR compared to everolimus, irrespective of MVD levels on both univariate and multivariate analysis **(Table 5, Figure 9a-b, Figure 10a-b Table 6).**

Table 5. Treatment comparison on PFS and OS by MVD and MCD levels (dichotomized at the upper 33% value) by treatment arm

	CABOZANTINIB (N=175)		EVEROLIMUS (N=185)		CABOZANTINIB vs EVEROLIMUS			
	N of events/ N patients	Months, Median (95% CI)	N of events/ N patients	Months, Median (95% CI)	Hazard ratio- Adjusted* (C vs E) (95%CI)	p-interaction	Hazard ratio- Unadjusted* (C vs E) (95%CI)	p-interaction
Microvascular density								
PFS								
Low (≤208.2 mm^2)	65/112	7.26 (5.52-7.49)	89/128	3.75 (3.58 -4.53)	0.45 (0.32-0.64)	*0.4961*	0.47 (0.34-0.65)	*0.3639*
High (>208.2 mm^2)	32/63	8.97 (6.28-NR)	34/57	7.26 (4.11-9.13)	0.56 (0.34-0.91)		0.62 (0.38-0.99)	
Adj HR (High vs Low)*		0.77 (.50-1.18)		0.63 (0.42-0.95)				
OS								
Low (≤208.2 mm^2)	49/112	20.76 (17.08-NR)	72/128	16.43 (13.24-18.89)	0.61 (0.42-0.89)	*0.7628*	0.69 (0.48-0.99)	*0.7745*

High (>208.2 mm^2)	21/63	NR (18.17-NR)	27/57	20.37 (13.93-NR)	0.55 (0.31-0.97)		0.62 (0.35-1.10)	
Adj HR (High vs Low)*		0.75 (.45-1.26)		0.84 (0.54-1.31)				
Mast cell Density								
PFS								
Low (≤11.3 mm^2)	60/102	7.16 (5.55-8.54)	82/114	3.75 (3.61-4.67)	0.43 (0.30-0.60)	*0.1127*	0.44 (0.32-0.62)	*0.1121*
High (>11.3 mm^2)	27/57	7.46 (7.23-NR)	27/52	7.49 (5.59-9.17)	0.71 (0.41-1.22)		0.74 (0.44-1.26)	
Adj. HR (High vs Low)*		0.85 (0.54-1.34)		0.51 (0.32-0.79)				
OS								
Low (≤11.3 mm^2)	43/102	20.07 (17.35-NR)	67/114	15.38 (11.60-18.80)	0.52 (0.35-0.77)	*0.2406*	0.59 (0.40-0.87)	*0.3691*
High (>11.3 mm^2)	19/57	NR (17.22-NR)	20/52	NR (16.23-NR)	0.82 (0.43-1.54)		0.83 (0.44-1.55)	
Adj. HR (High vs Low)*		0.88 (0.51-1.52		0.56 (0.34-0.94)				

Figure 9a: Kaplan Meier Curves of PFS by MVD or MCD Levels for Treatment Group Comparison. a) MVD Low Group, b) MVD high Group

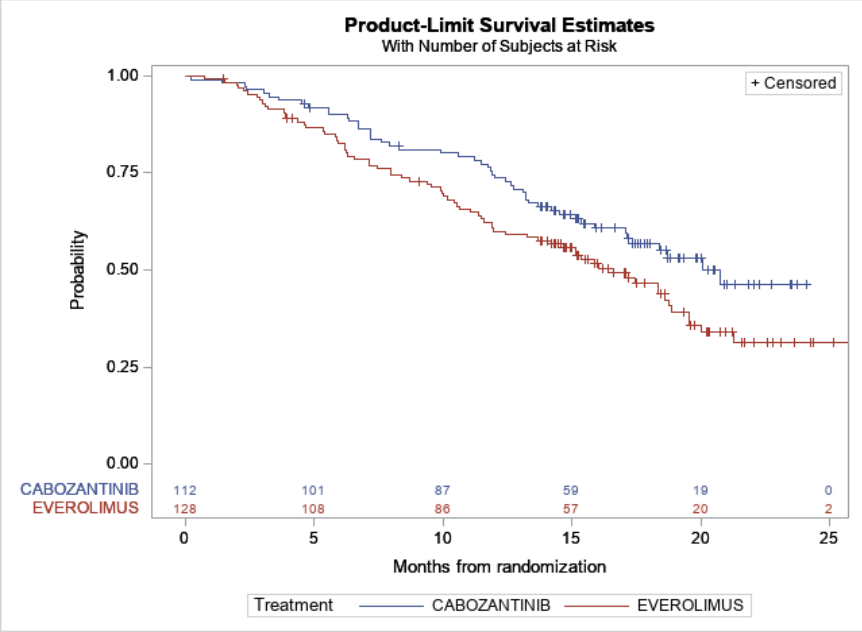

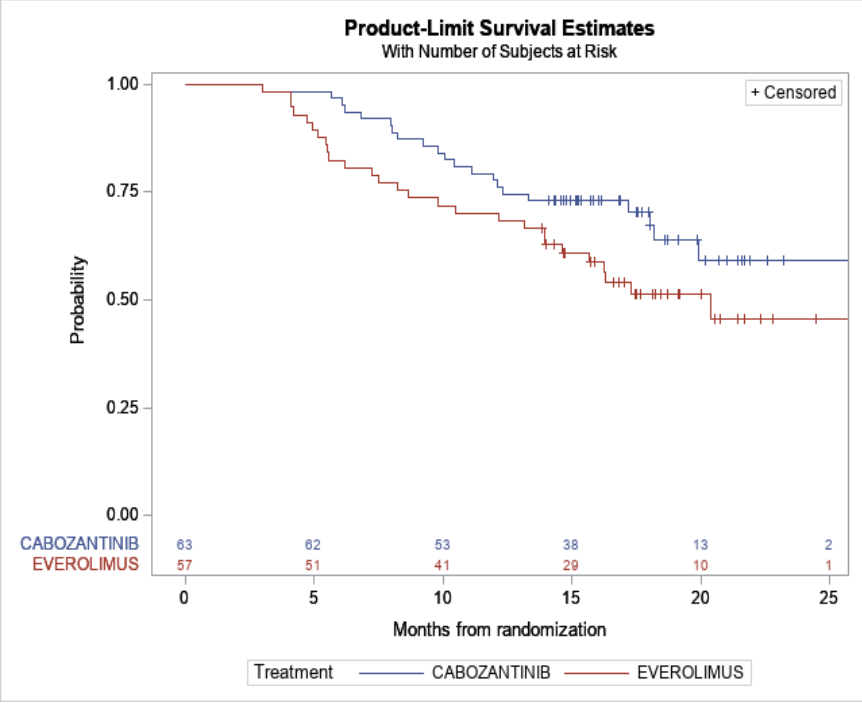

Figure 10 a-b. Kaplan Meier Curves of OS by MVD and MCD Levels for Treatment Group Comparison. a) MVD Low Group, b) MVD high Group

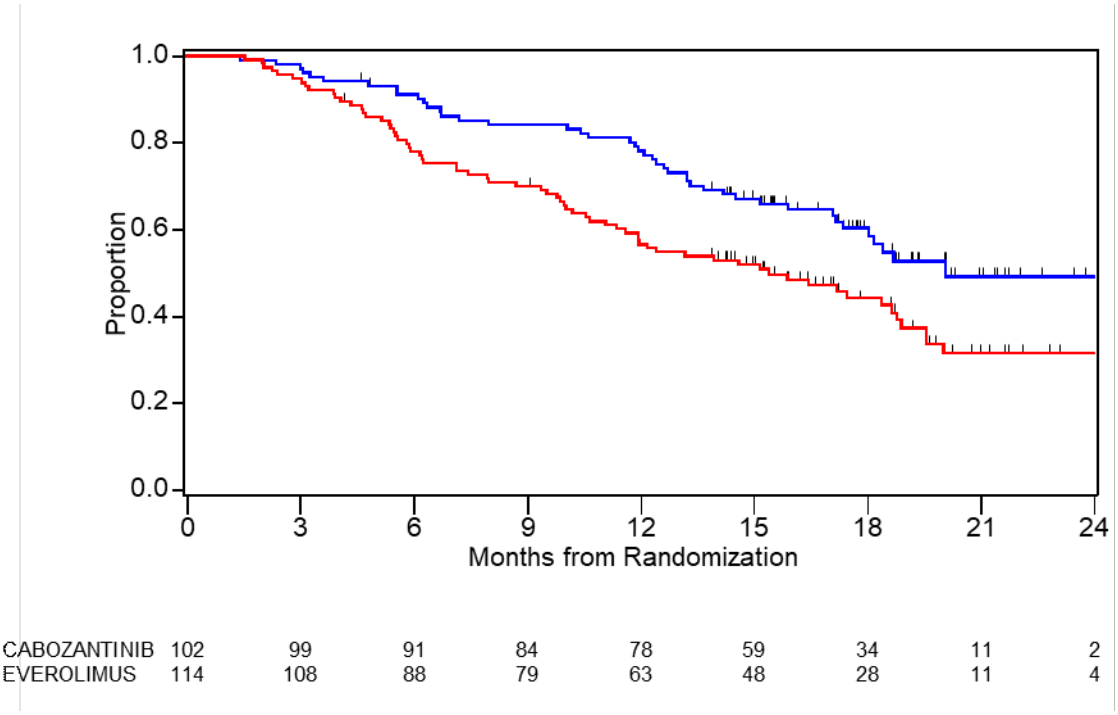

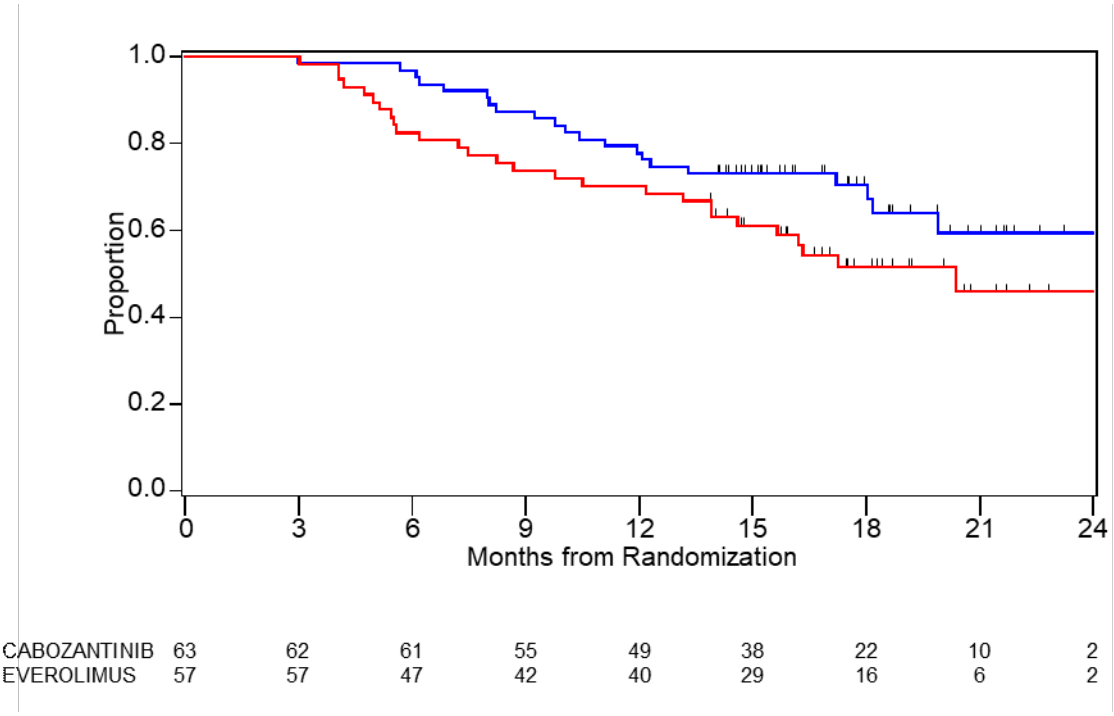

Table 6. Association of MVD and MCD with ORR and DCR by Treatment arm.

	CABOZANTINIB (N=175)		**EVEROLIMUS (N=185)**		**CABOZANTINIB vs EVEROLIMUS**	
Microvascular density						
ORR	**N ORR/TOTAL**	**ORR (%)**	**N ORR/TOTAL**	**ORR (%)**	**Odds Ratio (OR) (95% CI)**	**p-interaction**
Low	18/112	16	6/128	5	3.89 (1.49-10.19)	*0.7593*
High	10/63	16	2/57	4	5.19 (1.09-24.80)	
DCR	**N DCR/TOTAL**	**DCR (%)**	**N DCR/TOTAL**	**DCR (%)**		
Low	92/112	82	79/128	62	2.85 (1.57-5.20)	*0.7228*
High	54/63	86	41/57	72	2.34 (0.94-5.83)	
Mast cell density						
ORR	**N ORR/TOTAL**	**ORR (%)**	**N ORR/TOTAL**	**ORR (%)**	**Odds Ratio (OR) (95% CI)**	**P- interaction**
High	7/57	12	2/52	4	3.50 (0.69- 17.68)	0.9196
Low	18/102	18	6/114	5	3.86 (1.47-10.14)	
DCR	**N DCR/TOTAL**	**DCR (%)**	**N DCR/TOTAL**	**DCR (%)**		
High	49/57	86	38/52	73	2.26 (0.86-5.93)	0.7506
Low	84/102	82	`72/114	63	2.72 (1.44-5.14)	

Moreover, analysis of clinical outcome by MVD status in each treatment arm revealed that while everolimus-treated patients with high MVD had longer median PFS compared to patients with low MVD (7.3 months vs 3.8 months; adjusted HR 0.63; 95% CI 0.42-0.95), no association between PFS and MVD status was not observed in the cabozantinib arm **(Table 5)**. MVD was not associated with ORR, DCR **(Table 6)** or OS **(Table 5)** in either the cabozantinib or the everolimus arm.

Association of mast cell density with clinical outcomes

Intratumoral MC infiltration has been associated with angiogenesis in the context of ccRCC, but its prognostic and predictive value remains unknown. Therefore, we first tested for an association between MCD and clinical outcome in our patient cohort. Similar to MVD data analysis, patients were initially divided into low, medium and high MCD groups using tertile cut-points, but since the low and medium tertile groups displayed similar association with outcomes (**Figure 11c-d**), the upper tertile cut-point was selected to categorize patients in MCD-high and MCD-low dichotomous groups.

Figure 11. Kaplan Meier Curves of PFS and OS by MVD and MCD tertile groups, c) PFS by MCD tertile groups d) OS by MCD tertile groups

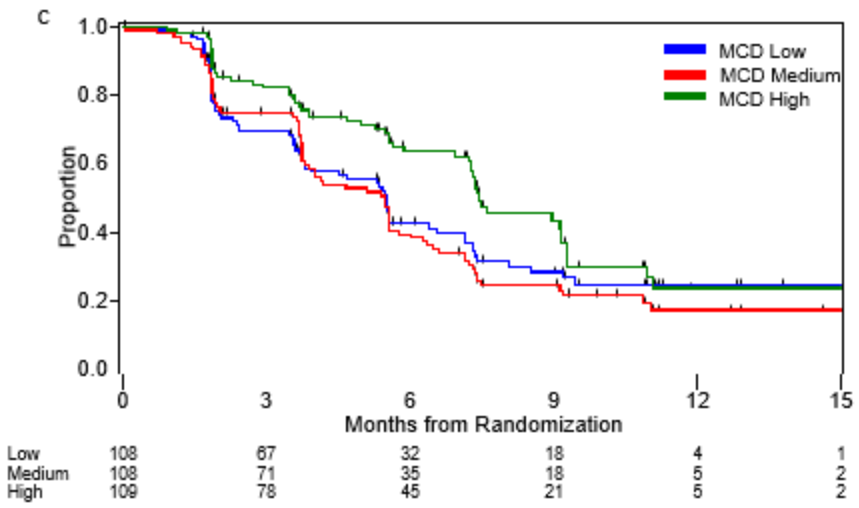

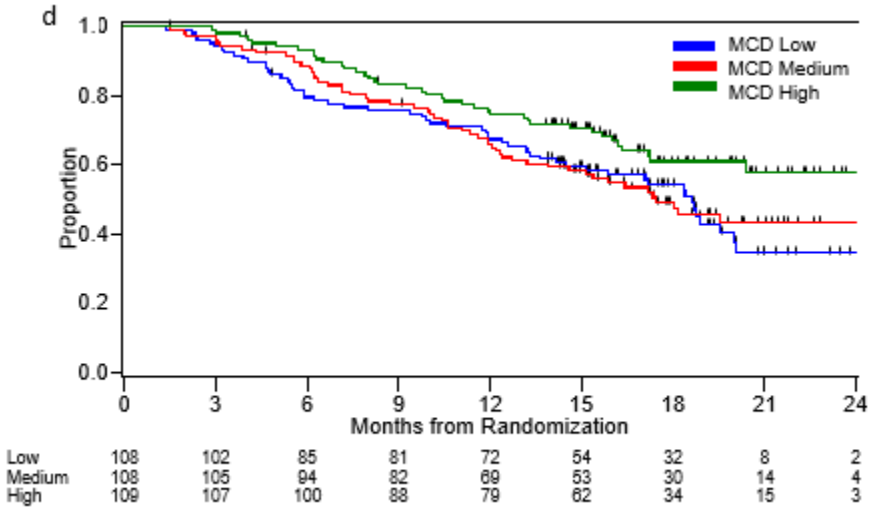

On univariate analysis, both median PFS and OS were significantly longer in patients with high MCD compared with patients with low MCD (PFS: 7.5 vs 5.5 months, HR 0.64; 95% CI 0.47-0.87; OS: NR vs 18.4 months, HR 0.66; 95% CI 0.44-0.92) **(Figure 12)**. Similar results were observed on multivariate analysis for both PFS (adjusted HR 0.66; 95% CI 0.48-0.91) and OS

(adjusted HR 0.69; 95% CI 0.48-0.99) **(Table 3)**. There was no association between MCD and DCR or ORR **(Table 4)**.

Figure 12. Kaplan Meier Curves of PFS and OS by MVD and MCD levels (dichotomous by upper 33% percentile) and of PFS by MCD groups and OS by MCD groups

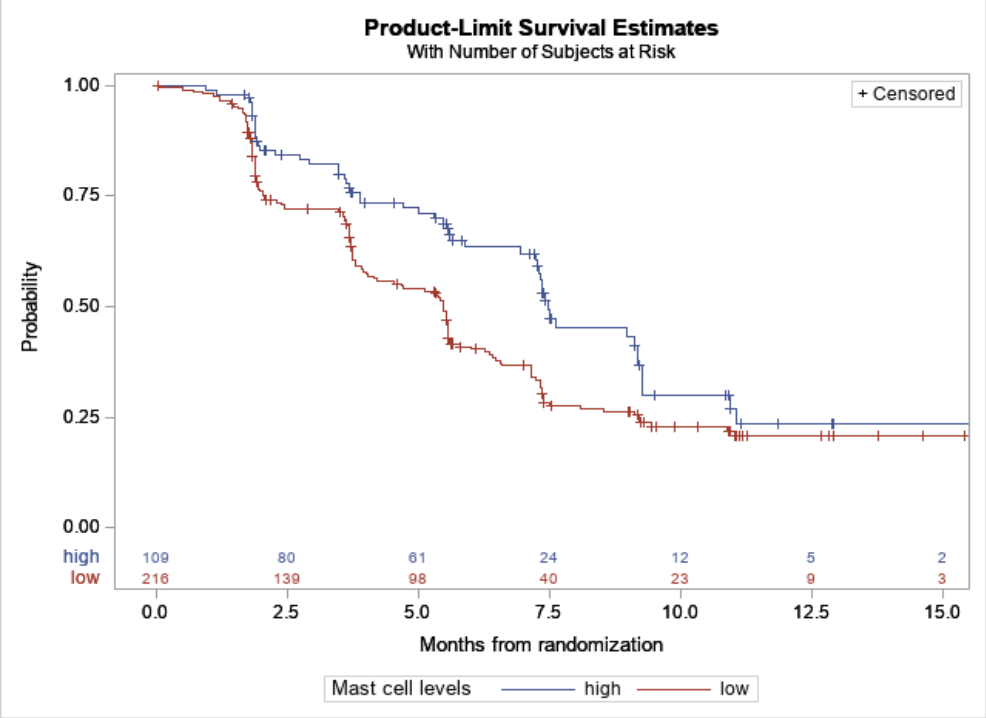

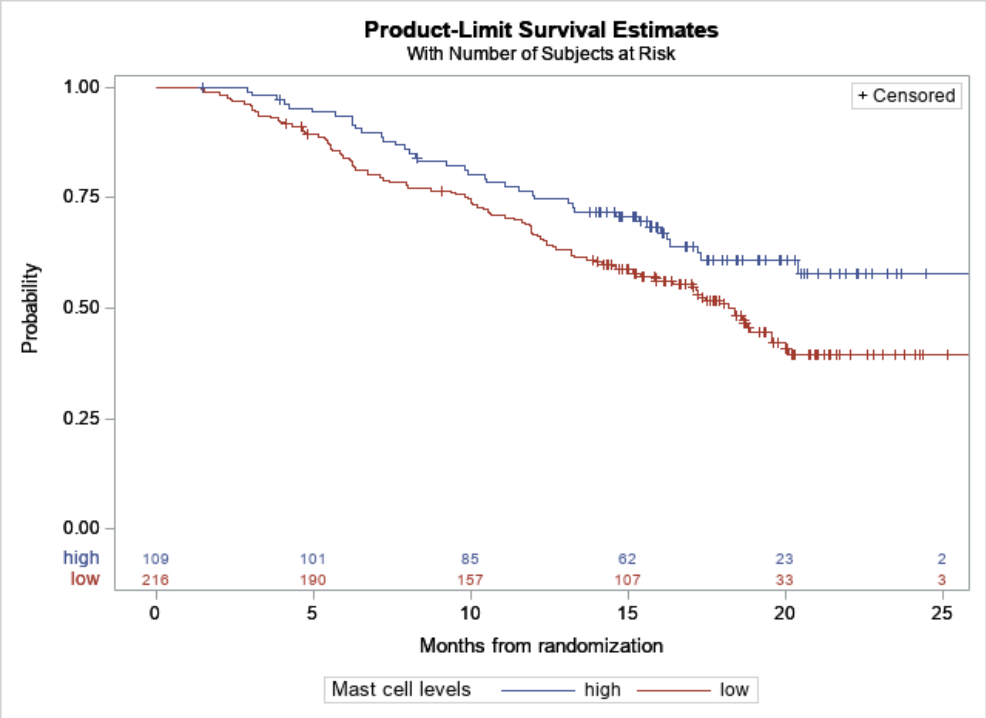

We then assessed the predictive value of MCD by comparing outcomes on cabozantinib versus everolimus in patients with high and low MCD. Treatment with cabozantinib was associated with improved ORR, and DCR compared to everolimus, irrespective of MCD levels on both univariate and multivariate analysis **(Table 6)**. For PFS and OS, however, the magnitude of treatment effect for cabozantinib versus everolimus tended to be greater in MCD-low group compared to MCD-high group, though the interaction test was not significant (p-interaction=0.112 for PFS and p-interaction=0.24 for OS) **(Table 4, Figure 13, Figure 14 a-b).**

Figure 13 Kaplan Meier Curves of PFS by MVD or MCD Levels for Treatment Group Comparison c) MCD Low Group, d) MCD high Group.

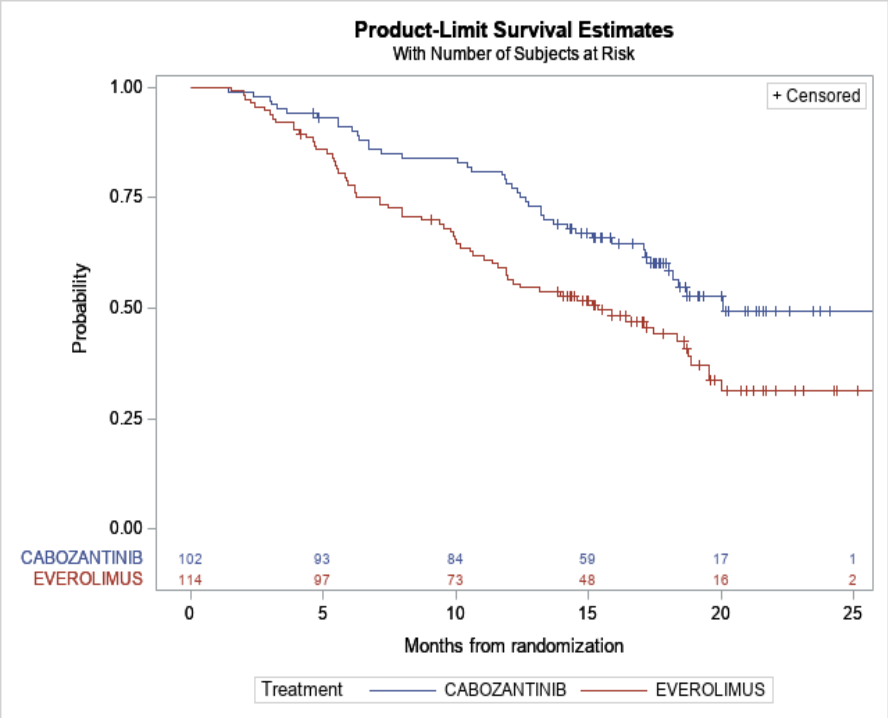
Product-Limit Survival Estimates
With Number of Subjects at Risk
+ Censored
1.00
0.75
0.50
0.25
0.00
Probability
CABOZANTINIB 102 93 84 59 17 1
EVEROLIMUS 114 97 73 48 16 2
0 5 10 15 20 25
Months from randomization
Treatment CABOZANTINIB EVEROLIMUS

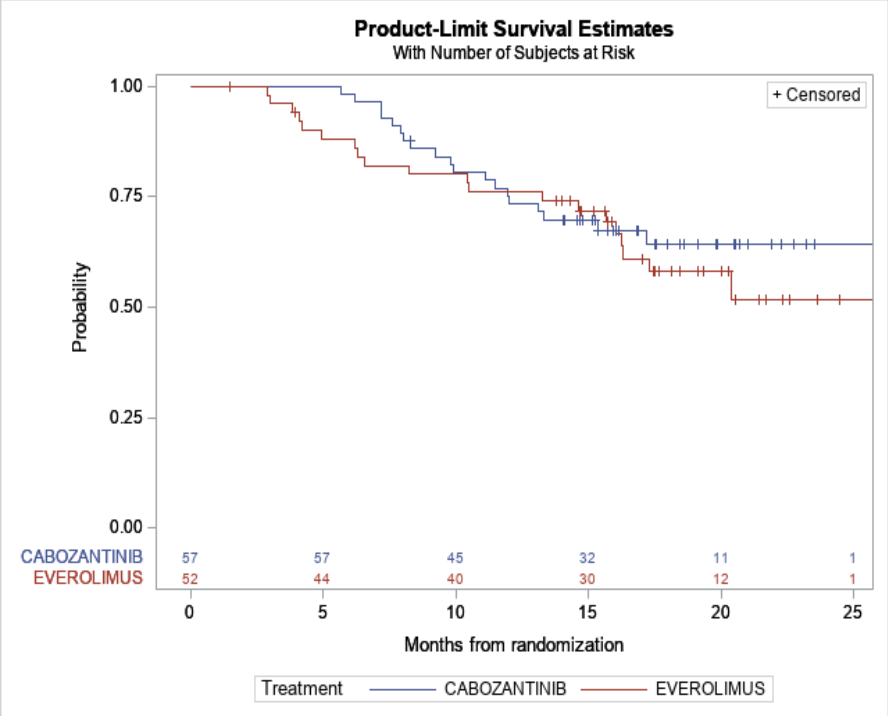
Product-Limit Survival Estimates
With Number of Subjects at Risk
+ Censored
1.00
0.75
0.50
0.25
0.00
Probability
CABOZANTINIB 57 57 45 32 11 1
EVEROLIMUS 52 44 40 30 12 1
0 5 10 15 20 25
Months from randomization
Treatment CABOZANTINIB EVEROLIMUS

Figure 14. Kaplan Meier Curves of OS by MVD and MCD Levels for Treatment Group Comparison. a) MCD Low Group, b) MCD high Group

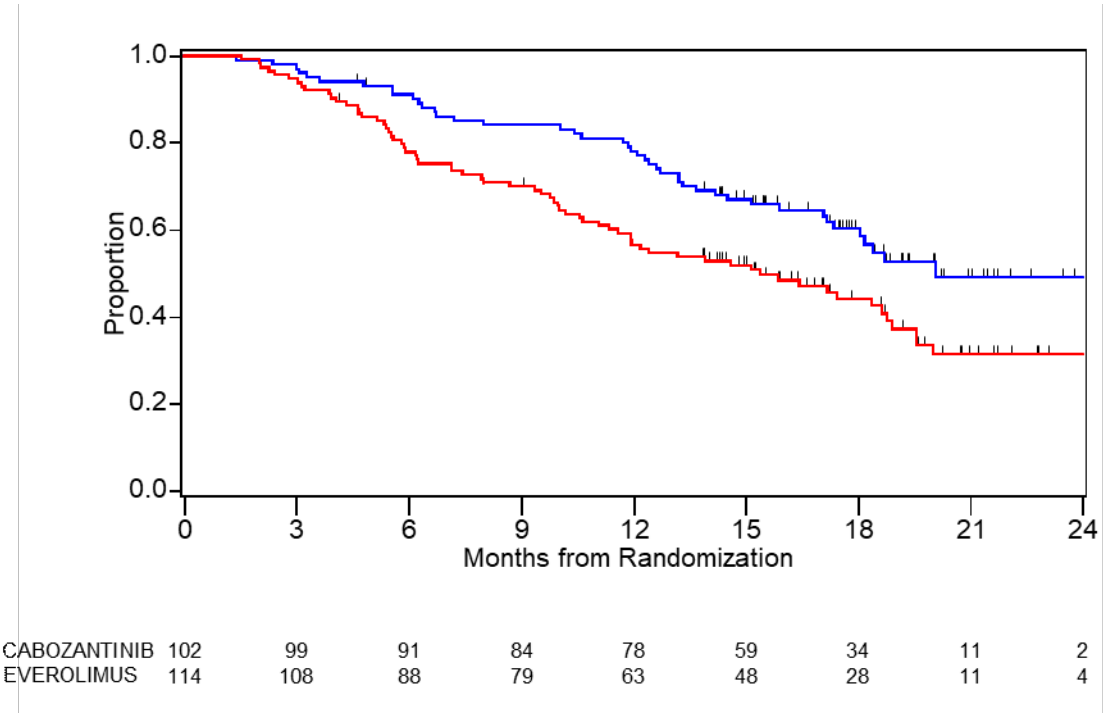

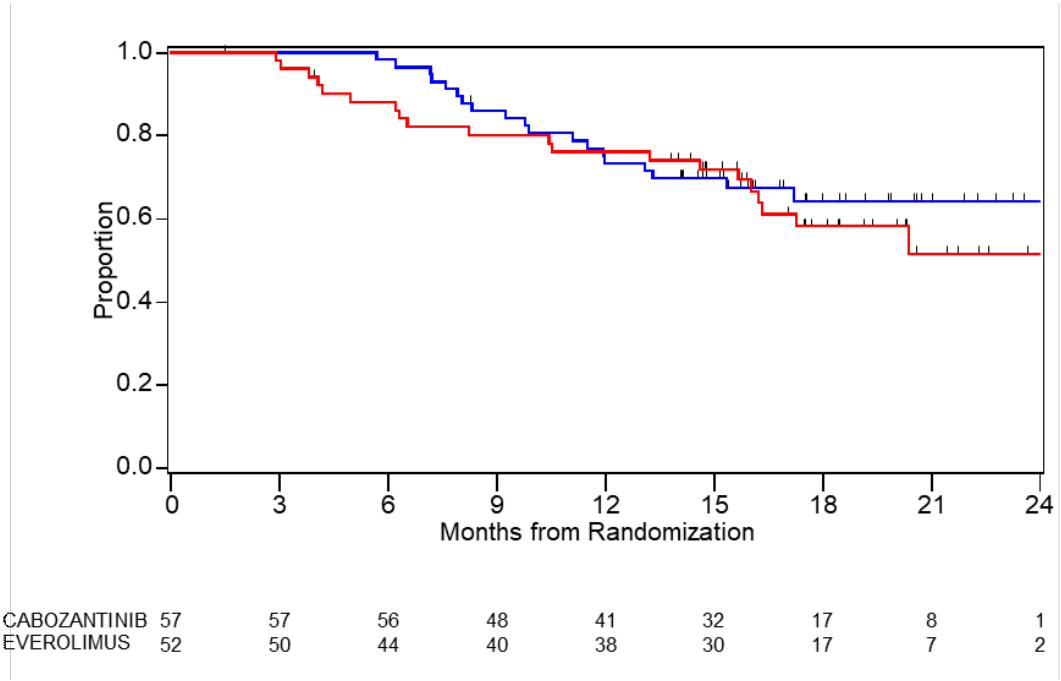

When we tested for an association between MCD and clinical outcome within each treatment arm, we found that in the everolimus arm, patients with high MCD had significantly longer median PFS and OS than patients with low MCD (PFS: 7.5 months vs 3.8 months; adjusted HR 0.51; 95% CI 0.32-0.79 and OS: NR vs 15.4 months; adjusted HR 0.56; 95% CI 0.34-0.94). In contrast, no association between MCD and PFS or OS was detected in the cabozantinib arm **(Table 4)**. MCD was not associated with ORR or DCR in either the cabozantinib or the everolimus arm **(Table 6)**.

Association of combined microvascular density and mast cell density with clinical outcomes

We further investigated the prognostic and predictive role of the two markers by stratifying patients in three groups according to dichotomous MVD levels combined with dichotomous MCD levels. Patients with high levels of either MCD or MVD (high/low or low/high) had significantly longer PFS compared to patients with low levels of both markers (MVD-low/MCD-low) (6.5 months vs 4.7 months; adjusted HR 0.69, 95% CI 0.49-0.97). Improved PFS was most evident in patients with high levels in both MCD and MVD (MVD-high/MCD-high) versus MVD-low/MCD-low patients (9.1 months vs 4.7 months; adjusted HR 0.57, 95% CI 0.38-0.85) **(Figure 1e, Table 7)**. No difference in ORR, DCR and OS was observed among the three patient groups identified by combined MVD/MCD levels **(Figure 1f, Tables 7 and 8)**.

Figure 15. Kaplan Meier Curves of PFS by MVD & MCD combination groups, and OS by MVD & MCD combination groups

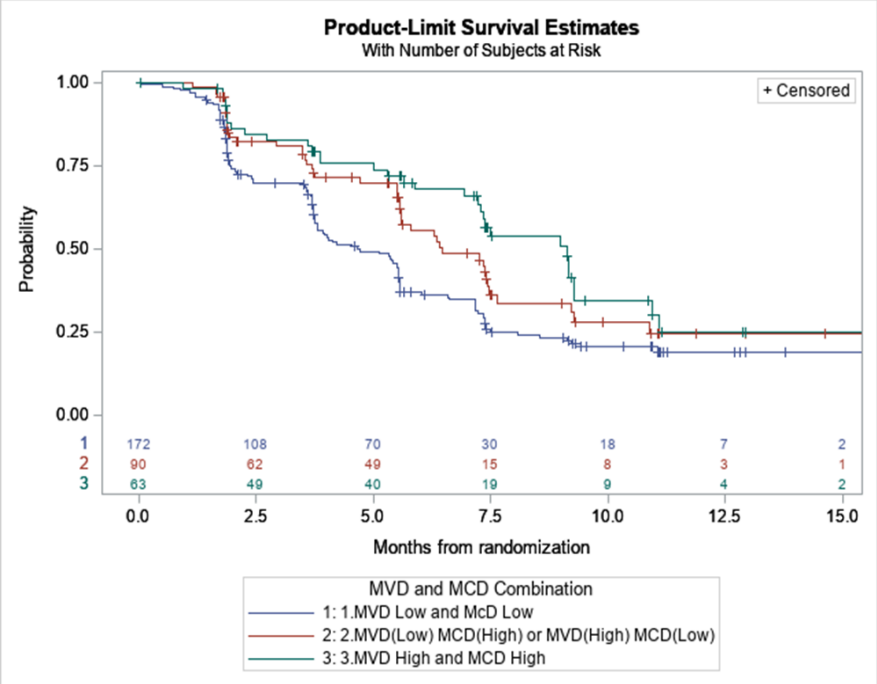

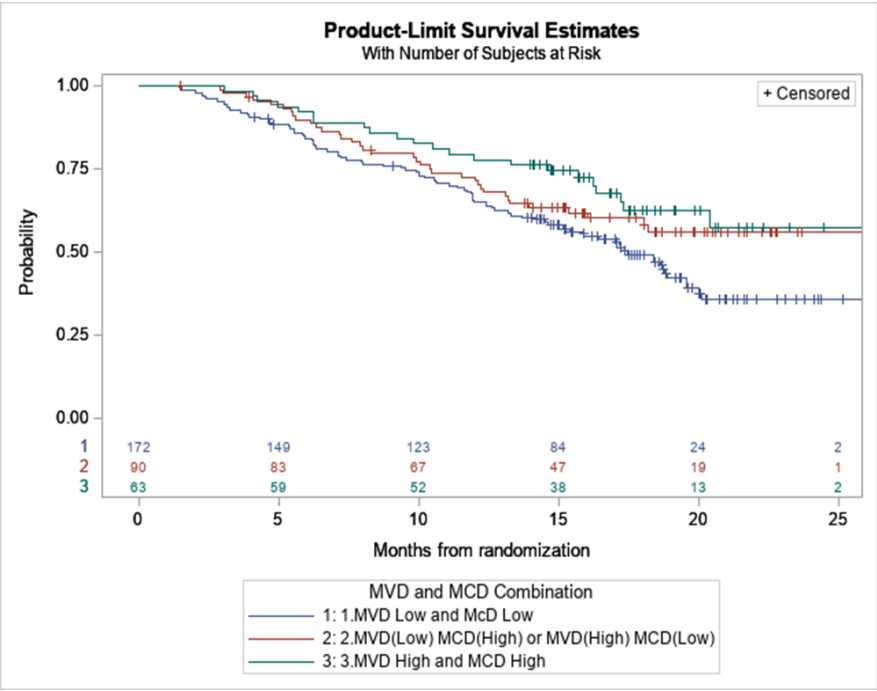

Tables 7. Association of MCD and MVD analyzed as three groups with PFS and OS

			Multivariable Analysis	
	N events/Total	**Month, Median (95% CI)**	**Adjusted* HR (95% CI)**	**p-value***
OS				
MVD Low and MCD Low	91/172	17.45 (15.16-19.55)	*reference*	
MVD (Low) MCD (High) or MVD (High) MCD (Low)	36/90	NR (16.03-NR)	0.72 (0.49-1.06)	*0.0986*
MVD High and MCD High	22/63	NR (17.28-NR)	0.66 (0.41-1.06)	*0.0821*
PFS				
MVD Low and MCD Low	117/172	4.70 (3.75-5.52)	*reference*	
MVD (Low) MCD (High) or MVD (High) MCD (Low)	47/90	6.47 (5.59-7.46)	0.69 (0.49-0.97)	*0.0316*
MVD High and MCD High	32/63	9.13 (7.23-9.26)	0.57 (0.38-0.85)	*0.0058*

Table 8. Association of MVD and MCD combination levels with ORR and DCR

ORR	**N ORR/Total**	**ORR %**
MVD Low and MCD Low	16/172	9%
MVD (Low) MCD (High) or MVD (High) MCD (Low)	14/90	16%
MVD High and MCD High	3/63	5%
p-value*		*0.6497*
DCR	**N DCR/Total**	**DCR %**

MVD Low and MCD Low	121/172	70%
MVD (Low) MCD (High) or MVD (High) MCD (Low)	73/90	81%
MVD High and MCD High	49/63	78%
p-value*		*0.1206*

*Cochran-Armitage Trend Test.

When the predictive value of the combined markers was assessed, treatment with cabozantinib was found to be associated with improved OS, ORR, and DCR compared to everolimus, irrespective of the combined MVD/MCD levels. For PFS, the magnitude of treatment effect for cabozantinib versus everolimus tended to be greater in MVD-low/MCD-low group, though the interaction test was not significant (p-interaction=0.261) **(Tables 9 and 10)**.

Table 9. Treatment comparison on PFS and OS by MCD and MVD levels

	CABOZANTINIB (N=159)		**EVEROLIMUS (N=166)**		**CABOZANTINIB vs EVEROLIMUS**		
	N events /N patients	**Months, Median (95% CI)**	**N events /N patients**	**Months, Median (95% CI)**	**Hazard ratio- Unadjusted (C vs E) (95%CI)**	**Hazard ratio- Adjusted (C vs E) (95%CI)**	**Adjusted p-interaction**
PFS							
G1: MVD Low and MCD Low	45/76	7.16 (5.49-8.54)	72/96	3.71 (2.30-4.21)	0.43 (0.30-0.63)	0.40 (0.27-0.59)	*0.2615*
G2: MVD (L) MCD (H) or MVD (H) MCD (L)	28/52	7.40 (5.78-9.26)	19/38	5.55 (3.70-7.39)	0.64 (0.36-1.15)	0.67 (0.37-1.21)	
G3: MVD High and MCD High	14/31	9.26 (5.30-NR)	18/32	9.13 (6.93-9.26)	0.70 (0.35-1.42)	0.64 (0.32-1.31)	
Unadj. HR (G2 vs G1)		0.89 (0.56-1.43)		0.60 (0.36-0.99)			
Unadj. HR (G3 vs G1)		0.68 (0.37-1.23)		0.42 (0.25-0.70)			

Adjusted HR (G2 vs G1)		0.96 (0.59-1.54)		0.58 (0.35-0.96)			
Adjusted HR (G3 vs G1)		0.72 (0.34-1.31)		0.45 (0.26-0.76)			
OS							
MVD Low and MCD Low	34/76	20.07 (15.90-NR)	57/96	15.89 (11.37-18.80)	0.65 (0.42-0.99)	0.54 (0.35-0.84)	*0.7961*
G2: MVD (L) MCD (H) or MVD (H) MCD (L)	19/52	NR (18.04-NR)	17/38	NR (10.45-NR)	0.65 (0.34-1.26)	0.70 (0.36-1.37)	
MVD High and MCD High	9/31	NR (17.22-NR)	13/32	20.40 (16.23-NR)	0.71 (0.31-1.67)	0.66 (0.28-1.54)	
Unadj.HR (G2 vs G1)		0.76 (0.43-1.33)		0.75 (0.44-1.30)			
Unadj. HR (G3 vs G1)		0.61 (0.29-1.30)		0.55 (0.30-1.00)			
Adjusted HR (G2 vs G1)		0.89 (0.50-1.56)		0.68 (0.39-1.18)			
Adjusted HR (G3 vs G1)		0.74 (0.35-1.56)		0.61 (0.34-1.13)			

Table 10. Association of MVD and MCD combination levels with ORR and DCR by treatment arm

	CABOZANTINIB (N=159)		**EVEROLIMUS (N=166)**		**CABOZANTINIB vs EVEROLIMUS**	
ORR	**N ORR/Total**	**ORR %**	**N ORR/Total**	**ORR %**	**Odds Ratio (OR) (95% CI)**	**p-interaction**
MVD Low and MCD Low	12/76	16	4/96	4	4.31 (1.33-13.97)	NE*
MVD (Low) MCD (High) or MVD (High) MCD (Low)	10/52	19	4/38	11	2.02 (0.58-7.03)	
MVD High and MCD High	3/31	10	0/32	0	NE*	
DCR	**N DCR/Total**	**DCR %**	**N DCR/Total**	**DCR %**		
MVD Low and MCD Low	62/76	82	59/96	61	2.78 (1.37-5.65)	0.8976
MVD (Low) MCD (High) or MVD (High) MCD (Low)	45/52	87	28/38	74	2.30 (0.78-6.73)	

MVD High and MCD High	26/31	84	23/32	72	2.04 (0.60-6.95)	

*NE=Not evaluable as G3 group has 0 event for ORR.

Analysis of clinical outcome by combined MVD/MCD status in each treatment arm showed that in the everolimus arm both PFS and OS were significantly longer in MVD-high/MCD-high patients compared to MVD-low/MCD-low patients (PFS: 9.1 months vs 3.7 months; adjusted HR 0.45, 95% CI 0.26-0.76 and OS: 20.4 months vs 15.9 months; adjusted HR 0.61, 95% CI 0.34-1.13); only PFS was significantly longer in patients with high levels of either MCD or MVD (high/low or low/high) compared to MVD-low/MCD-low patients (PFS: 5.5 months vs 3.7 months; adjusted HR 0.58, 95% CI 0.35-0.96). Conversely, no association between combined MVD/MCD levels and PFS or OS was observed in the cabozantinib arm. No difference in ORR and DCR was observed among the three patient groups identified by combined MVD/MCD levels in either the cabozantinib or the everolimus arm **(Tables 9 and 10)**.

Association of Met expression combined with microvascular density or mast cell density with clinical outcomes.

As Met is one of targets of cabozantinib, we explored the impact of its expression (previously assessed by IHC)[60] combined with MVD or MCD on clinical outcomes.

To analyze combined expression of Met and MVD we considered two main groups (due to the small number of patients in some subgroups): 1) patients without expression of Met and low MVD (MVDlow/Met-negative), 2) patients with either Met expression, or high MVD, or both (MVDhigh and/or Met-positive). Improved PFS on cabozantinib relative to everolimus was observed in both in MVDlow/Met-negative and MVDhigh and/or Met-positive patients. Similar results were observed for ORR and DCR **(Tables 11 and 12)**. For OS, the magnitude of treatment effect for cabozantinib versus everolimus tended to be greater for MVDhigh and/or Met-positive patients compared to MVDlow/Met-negative patients, though the interaction test was not significant (p-interaction=0.20) **(Table 11)**.

Table 11. Treatment comparison on PFS and OS by MVD or MCD and MET combination levels by treatment arm

	CABOZANTINIB (N=123)		**EVEROLIMUS (N=131)**		**CABOZANTINIB vs EVEROLIMUS**		
	N events/ N patients	**Months, Median (95% CI)**	**N events /N patients**	**Months, Median (95% CI)**	**Hazard ratio- Unadjusted (C vs E) (95%CI)**	**Hazard ratio- Adjusted (C vs E) (95%CI)**	**Adjusted p-interaction**
Microvascular density							
PFS							
G1. MVD/MET: -/-	35/57	7.16 (5.52- 9.13)	43/65	3.91 (2.92-5.13)	0.54 (0.35-0.85)	0.54 (0.34-0.86)	*0.4706*
G2. MVD/MET: +/-, -/+, +/+	33/66	8.54 (6.28-NR)	44/66	5.32 (3.68-7.16)	0.48 (0.30-0.75)	0.43 (0.27-0.68)	
Unadjusted HR (G2 vs G1)		0.77 (0.48-1.24)		0.88 (0.58-1.35)			

Adjusted HR (G2 vs G1)		0.77 (0.47-1.24)		0.97 (0.63-1.51)			
OS							
G1. MVD/MET: -/-	26/57	18.69 (15.34-NR)	36/65	17.18 (11.93-18.89)	0.75 (0.45-1.24)	0.73 (0.44-1.22)	*0.2035*
G2. MVD/MET: +/-, -/+, +/+	21/66	NR (NR-NR)	33/66	16.33 (11.96-NR)	0.51 (0.29-0.88)	0.45 (0.26-0.78)	
Unadjusted HR (G2 vs G1)		0.65 (0.37-1.16)		0.96 (0.59-1.53)			
Adjusted HR (G2 vs G1)		0.68 (0.38-1.21)		1.10 (0.68-1.79)			
Mast-cell density							
PFS							
G1. MCD/MET -/-	35/53	5.78 (5.49-8.08)	44/64	4.04 (3.58-5.55)	0.60 (0.38-0.92)	0.55 (0.35-0.88)	*0.5283*
G2. MCD/MET +/-, -/+, +/+	26/57	9.26 (7.33-NR)	32/52	5.49 (3.71-7.62)	0.49 (0.29-0.83)	0.44 (0.26-0.76)	
Unadjusted HR (G2 vs G1)		0.64 (0.38-1.06)		0.76 (0.48-.21)			

Adjusted HR (G2 vs G1)		0.64 (0.38-1.08)		0.80 (0.50-1.27)			
OS							
G1. MCD/MET -/-	24/53	20.07 (15.9-NR)	35/64	17.18 (11.93-19.55)	0.72 (0.43-1.21)	0.70 (0.41-1.18)	*0.3916*
G2. MCD/MET +/-, -/+, +/+	18/57	NR (18.17-NR)	24/52	17.28 (10.18-NR)	0.55 (0.30-1.01)	0.49 (0.27-0.91)	
Unadjusted HR (G2 vs G1)		0.69 (0.37-1.27)		0.90 (0.54-1.52)			
Adjusted HR (G2 vs G1)		0.71 (0.38-1.32)		1.00 (0.59-1.70)			

Similar to MVD/Met analysis, evaluation of combined MCD/Met data was conducted by grouping patients with low MCD and negative Met expression, and comparing them to patients with either high MCD, or positive Met expression, or both. Treatment with cabozantinib was found to be associated with improved PFS, OS, ORR, and DCR compared to everolimus both in MCDlow/ Met-negative patients and in MCDhigh and/or Met-positive patients **(Tables 11 and 12)**.

Table 12. MVD or MCD and MET combination levels with ORR and DCR by treatment arm

	CABOZANTINIB (N=123)		**EVEROLIMUS (N=131)**		**CABOZANTINIB vs EVEROLIMUS**	
Microvascular density						
ORR	**N ORR/Total**	**ORR %**	**N ORR/Total**	**ORR %**	**Odds Ratio (OR) (95% CI)**	**p-interaction**
G1. MVD/MET: -/-	13/57	23	4/65	6	4.51 (1.38-14.75)	*0.7385*
G2. MVD/MET: +/-, -/+, +/+	9/66	14	3/66	5	3.32 (0.86-12.85)	
DCR	**N DCR/ N Patients**	**DCR %**	**N DCR/ N Patients**	**DCR %**		
G1. MVD/MET: -/-	50/57	88	42/65	65	3.91 (1.53-10.02)	*0.9843*
G2. MVD/MET: +/-, -/+, +/+	57/66	87	41/66	62	3.86 (1.63-9.14)	
Mast cell density						

ORR	N ORR/Total	ORR %	N ORR/Total	ORR %	Odds Ratio (OR) (95% CI)	p-interaction
G1. MCD/MET -/-	11/53	21	6/64	9	2.53 (0.87-7.39)	*0.3251*
G2. MCD/MET +/-, -/+, +/+	8/57	14	1/52	2	8.33 (1.00- 69.06)	
DCR	**N DCR/ N Patients**	**DCR %**	**N DCR/ N Patients**	**DCR %**		
G1. MCD/MET -/-	44/53	83	42/64	66	2.56 (1.06-6.19)	*0.3462*
G2. MCD/MET +/-, -/+, +/+	51/57	90	33/52	63	4.89 (1.77- 13.53)	

Discussion

Our analyses of tumor tissue samples from the METEOR trial showed that high levels of tumor angiogenesis markers (including MVD and MCD) are associated with longer PFS in the entire patient cohort. However, when the treatment arms were analyzed separately, this association continued to be observed among patients treated with everolimus but not among patients treated with cabozantinib. Moreover, the PFS improvement with cabozantinib versus everolimus tended to be greater in patients with low levels of tumor angiogenesis markers. These results are at odds with recent results from several clinical trial cohorts consistently showing that in sunitinib-treated patients, high levels of tumor angiogenesis (measured by an angiogenesis signature) are associated with better clinical outcome[33–35].

Sunitinib is a potent inhibitor of VEGFR, platelet-derived growth factor receptor (PDGFR), and c-Kit and preclinical data demonstrated that it exerts both anti-angiogenesis and anti-tumor effects[110]. In xenograft models of ccRCC, sunitinib was shown to dramatically reduce tumor vascularization and induce tumor cell necrosis[111,112]. In patients with mccRCC treated VEGFR TKIs (including sunitinib), an on-treatment decrease in arterial spin labeled (ASL) MRI perfusion was associated with tumor response[30]. Overall, these data suggest that in ccRCC, sunitinib acts primarily through an anti-angiogenic mechanism. The recent findings that sunitinib is more effective in mccRCC patients with a high angiogenic gene signature is in line with this hypothesis.

On the other hand, the mechanism of action of cabozantinib in kidney cancer has been unclear. Compared to sunitinib, cabozantinib is a more potent VEGFR2 inhibitor[39,40], raising the possibility that its higher efficacy in ccRCC is largely due to a stronger inhibition of tumor

vascularity. However, cabozantinib inhibits additional RTKs, including Met and Axl, which are known to play an important role in ccRCC biology and have been implicated in cell growth invasion, invasion metastasis, angiogenesis, and resistance to sunitinib therapy[39,113–115]. Our findings that (contrary to sunitinib) cabozantinib is highly effective in mccRCC patients with low levels of tumor angiogenesis strongly suggest that its mechanism of action cannot be simply ascribed to its potent VEGFR2 inhibition but likely involves tumor intrinsic inhibition of Met, Axl, and potentially other RTKs. Our finding that OS improvement with cabozantinib versus everolimus tends to be greater for patients with high MVD and/or Met-positive tumors compared to patients with both low MVD and Met-negative tumors seems to support this possibility. Given that cabozantinib displays a high-spectrum of activity against multiple signaling pathways, the identification of predictors of response likely requires the development of a combined multi-marker model; such model might need to integrate genomic-, transcriptomic-, and protein-based biomarkers. As preclinical studies have also suggested a possible immunomodulatory function of cabozantinib in RCC[116], future investigations should also include an in-depth characterization of the tumor microenvironment.

In this work, we confirmed the presence of a strong correlation between MVD and MCD in ccRCC, as previously reported[102,104]. Moreover, we demonstrated that both MVD and MCD are negatively associated with tumor grade. These findings are consistent with previously published results from the ECOG-ACRIN 2805 trial demonstrating that in localized high risk RCC, high levels of angiogenesis (measured by MVD) are associated with favorable histopathologic features and improved OS[109]. Similar to MVD, high MCD was also previously reported as good prognostic factor in non-metastatic ccRCC[117]. Along these lines, we found that

in patients treated with everolimus, both high MVD and high MCD were associated with longer PFS, and high MCD was also associated with longer OS. It is uncertain, however, whether these results simply reflect the indolent clinical behavior of high-angiogenic tumors or might be also linked to a possible anti-angiogenic effect of MTOR inhibition.

Although MVD and high MCD were found to be highly correlated, the combination of the two biomarkers further stratified patient outcomes in the whole patient cohort and in the everolimus arm. Indeed, improved PFS was most evident in patients with high levels of both MCD and MVD. These data indicate that the role of MVD and MCD as biomarkers is not completely overlapping and suggest that tumor infiltrating mast cells may play a role in the tumor microenvironment that goes beyond the induction of angiogenesis[118].

This study presents several limitations. First, our analyses were performed in archival tissues that were mostly collected before the patients received any systemic therapy. Therefore, these samples are not representative of the changes in tumor biology that might have been induced by treatments received prior to cabozantinib. Second, the tissue slides used for immunohistochemistry were obtained from institutions worldwide, which likely have different tissue handling, fixation and processing protocols that differently affect the immunoreactivity of the samples. This is a general issue related to the analysis of clinical trial specimens that in our study was at least in part overcome by the fact that assessment of MVD and MCD did not require quantification of staining intensity, and thus less immunoreactive slides could be reliably analyzed as long as specific staining was present. Finally, our studies were conducted on a single tumor section per patient. While this approach does not fully address possible intratumoral heterogeneity, in order to mitigate this issue, we developed image analysis protocols that allowed us obtain data

from the whole tissue section rather than focusing on small selected regions of interest, as frequently done in tissue-based biomarker investigations.

Conclusions

Cabozantinib inhibits multiple tyrosine kinase receptors (RTKs), including VEGFRs, Met, and Axl, and is superior to VEGFR-inhibitors (i.e., sunitinib) in the treatment of metastatic clear cell renal cell carcinoma (mccRCC). However, it has been unclear whether its efficacy in kidney cancer is mainly due to anti-angiogenic effects mediated by its potent inhibition of VEGFRs or also involves tumor intrinsic targeting of additional RTKs. Using archival tumor samples from the METEOR trial, we demonstrated that, compared to everolimus, cabozantinib displays high efficacy in mccRCC regardless of the levels of tumor angiogenesis. Our findings suggest that cabozantinib might not simply work as an anti-angiogenic drug and that its mechanism of action involves the inhibition of multiple signaling pathways. This knowledge is critical for the future development of biomarkers of response to cabozantinib in mccRCC.

References

1. Siegel RL, Miller KD, Jemal A. Cancer statistics, 2018. *CA Cancer J Clin*. 2018;68(1):7-30.

2. Capitanio U, Montorsi F. Renal cancer. In: *The Lancet*. Vol 387. ; 2016:894-906.

3. MacLennan GT, Cheng L. Five decades of urologic pathology: the accelerating expansion of knowledge in renal cell neoplasia. *Hum Pathol*. 2020.

4. Cheng L, Zhang S, MacLennan GT, Lopez-Beltran A, Montironi R. Molecular and cytogenetic insights into the pathogenesis, classification, differential diagnosis, and prognosis of renal epithelial neoplasms. *Hum Pathol*. 2009.

5. Moch H, Cubilla AL, Humphrey PA, Reuter VE, Ulbright TM. The 2016 WHO Classification of Tumours of the Urinary System and Male Genital Organs—Part A: Renal, Penile, and Testicular Tumours. *Eur Urol*. 2016;70(1):93-105.

6. Motzer RJ, Jonasch E, Boyle S, et al. Kidney cancer, version 1.2021: Featured updates to the nccn guidelines. *JNCCN J Natl Compr Cancer Netw*. 2020;18(9):1160-1170.

7. Frew IJ, Moch H. A Clearer View of the Molecular Complexity of Clear Cell Renal Cell Carcinoma. *Annu Rev Pathol Mech Dis*. 2014;10(1):263-289.

8. Moch H, Montironi R, Lopez-Beltran A, Cheng L, Mischo A. Oncotargets in Different Renal Cancer Subtypes. *Curr Drug Targets*. 2015;16(2):125-135.

9. Ricketts CJ, De Cubas AA, Fan H, et al. The Cancer Genome Atlas Comprehensive

Molecular Characterization of Renal Cell Carcinoma. *Cell Rep*. 2018.

10. The Cancer Genome Atlas Research Network. Comprehensive Molecular Characterization of Papillary Renal-Cell Carcinoma. *N Engl J Med*. 2016;374(2):135-145.

11. Varela I, Tarpey P, Raine K, et al. Exome sequencing identifies frequent mutation of the SWI/SNF complex gene PBRM1 in renal carcinoma. *Nature*. 2011;469(7331):539-542.

12. Cimadamore A, Massari F, Santoni M, et al. Molecular characterization and diagnostic criteria of renal cell carcinoma with emphasis on liquid biopsies. *Expert Rev Mol Diagn*. 2020.

13. Marchetti A, Rosellini M, Mollica V, et al. The molecular characteristics of non-clear cell renal cell carcinoma: What's the story morning glory? *Int J Mol Sci*. 2021;22(12).

14. Cimadamore A, Cheng L, Scarpelli M, et al. Towards a new WHO classification of renal cell tumor: What the clinician needs to know-a narrative review. *Transl Androl Urol*. 2021;10(3):1506-1520.

15. George DJ, Kaelin WG. The von Hippel–Lindau Protein, Vascular Endothelial Growth Factor, and Kidney Cancer. *N Engl J Med*. 2003;349(5):419-421.

16. Gnarra JR, Tory K, Weng Y, et al. Mutations of the VHL tumour suppressor gene in renal carcinoma. *Nat Genet*. 1994;7(1):85-90.

17. Schödel J, Grampp S, Maher ER, et al. Hypoxia, hypoxia-inducible transcription factors, and renal cancer. *Eur Urol*. 2016;69(4):646-657.

18. Iliopoulos O, Levy AP, Jiang C, Kaelin WG, Goldberg MA. Negative regulation of

hypoxia-inducible genes by the von Hippel-Lindau protein. *Proc Natl Acad Sci U S A*. 1996;93(20):10595-10599.

19. Bacigalupa ZA, Rathmell WK. Beyond glycolysis: Hypoxia signaling as a master regulator of alternative metabolic pathways and the implications in clear cell renal cell carcinoma. *Cancer Lett*. 2020;489:19-28.

20. Escudier B, Porta C, Schmidinger M, et al. Renal cell carcinoma: ESMO Clinical Practice Guidelines for diagnosis, treatment and follow-up. *Ann Oncol*. 2019;30(5):706-720.

21. Cho H, Du X, Rizzi JP, et al. On-target efficacy of a HIF-2α antagonist in preclinical kidney cancer models. *Nature*. 2016;539(7627):107-111.

22. Davis CF, Ricketts CJ, Wang M, et al. The somatic genomic landscape of chromophobe renal cell carcinoma. *Cancer Cell*. 2014;26(3):319-330.

23. Powles T, Staehler M, Ljungberg B, et al. Updated EAU Guidelines for Clear Cell Renal Cancer Patients Who Fail VEGF Targeted Therapy. *Eur Urol*. 2016;69(1):4-6.

24. Motzer RJ, Escudier B, McDermott DF, et al. Nivolumab versus Everolimus in Advanced Renal-Cell Carcinoma. *N Engl J Med*. 2015;373(19):1803-1813.

25. Santoni M, Massari F, Aurilio G, et al. Designing novel immunocombinations in metastatic renal cell carcinoma. *Immunotherapy*. 2020;12(17).

26. Mollica V, Rizzo A, Di Nunno V, et al. Adjuvant therapy in renal cell carcinoma: Is it the right strategy to inhibit VEGF? *Transl Androl Urol*. 2021;10(3):1581-1587.

27. Santoni M, Heng DYC, Aurilio G, et al. Combining Radiotherapy with Immunocheckpoint

Inhibitors or CAR-T in Renal Cell Carcinoma. *Curr Drug Targets*. 2019;21(4):416-423.

28. Mollica V, Di Nunno V, Gatto L, et al. Novel Therapeutic Approaches and Targets Currently Under Evaluation for Renal Cell Carcinoma: Waiting for the Revolution. *Clin Drug Investig*. 2019.

29. Wilhelm SM, Carter C, Tang LY, et al. BAY 43-9006 exhibits broad spectrum oral antitumor activity and targets the RAF/MEK/ERK pathway and receptor tyrosine kinases involved in tumor progression and angiogenesis. *Cancer Res*. 2004;64(19):7099-7109.

30. Tsai LL, Bhatt RS, Strob MF, et al. Arterial Spin Labeled Perfusion MRI for the Evaluation of Response to Tyrosine Kinase Inhibition Therapy in Metastatic Renal Cell Carcinoma. *Radiology*. 2021;298(2):332-340.

31. Le Tourneau C, Raymond E, Faivre S. Sunitinib: A novel tyrosine kinase inhibitor. A brief review of its therapeutic potential in the treatment of renal carcinoma and gastrointestinal stromal tumors (GIST). *Ther Clin Risk Manag*. 2007;3(2):341-348.

32. Di Nunno V, Massari F, Mollica V, et al. Another one in the chamber: cabozantinib for patients with metastatic non clear cell renal cell carcinoma. *Ann Transl Med Publ Ahead Print*. 2019.

33. McDermott DF, Huseni MA, Atkins MB, et al. Clinical activity and molecular correlates of response to atezolizumab alone or in combination with bevacizumab versus sunitinib in renal cell carcinoma. *Nat Med*. 2018;24(6):749-757.

34. Motzer RJ, Banchereau R, Hamidi H, et al. Molecular Subsets in Renal Cancer Determine

Outcome to Checkpoint and Angiogenesis Blockade. *Cancer Cell*. 2020;38(6):803-817.e4.

35. Motzer RJ, Robbins PB, Powles T, et al. Avelumab plus axitinib versus sunitinib in advanced renal cell carcinoma: biomarker analysis of the phase 3 JAVELIN Renal 101 trial. *Nat Med*. 2020;26(11):1733-1741.

36. Choueiri TK, Escudier B, Powles T, et al. Cabozantinib versus everolimus in advanced renal cell carcinoma (METEOR): final results from a randomised, open-label, phase 3 trial. *Lancet Oncol*. 2016;17(7):917-927.

37. Choueiri TK, Halabi S, Sanford BL, et al. Cabozantinib versus sunitinib as initial targeted therapy for patients with metastatic renal cell carcinoma of poor or intermediate risk: The alliance A031203 CABOSUN trial. *J Clin Oncol*. 2017;35(6):591-597.

38. Choueiri TK, Powles T, Burotto M, et al. Nivolumab plus Cabozantinib versus Sunitinib for Advanced Renal-Cell Carcinoma. *N Engl J Med*. 2021;384(9):829-841.

39. Yakes FM, Chen J, Tan J, et al. Cabozantinib (XL184), a Novel MET and VEGFR2 Inhibitor, Simultaneously Suppresses Metastasis, Angiogenesis, and Tumor Growth. *Mol Cancer Ther*. 2011;10(12):2298-2308.

40. Choueiri TK, Kaelin WG. Targeting the HIF2–VEGF axis in renal cell carcinoma. *Nat Med*. 2020;26(10):1519-1530.

41. Iacovelli R, Nolè F, Verri E, et al. Prognostic Role of PD-L1 Expression in Renal Cell Carcinoma. A Systematic Review and Meta-Analysis. *Target Oncol*. 2016;11(2):143-148.

42. Motzer RJ, Tannir NM, McDermott DF, et al. Nivolumab plus Ipilimumab versus Sunitinib

in Advanced Renal-Cell Carcinoma. *N Engl J Med*. 2018;378(14):1277-1290.

43. Choueiri TK, Fishman MN, Escudier B, et al. Immunomodulatory activity of nivolumab in metastatic renal cell carcinoma. In: *Clinical Cancer Research*. Vol 22. ; 2016:5461-5471.

44. Rini BI, Plimack ER, Stus V, et al. Pembrolizumab plus Axitinib versus Sunitinib for Advanced Renal-Cell Carcinoma. *N Engl J Med*. 2019;380(12):1116-1127.

45. McDermott DF, Lee J-L, Szczylik C, et al. Pembrolizumab monotherapy as first-line therapy in advanced clear cell renal cell carcinoma (accRCC): Results from cohort A of KEYNOTE-427. *J Clin Oncol*. 2018;36(15_suppl):4500-4500.

46. McDermott DF, Lee J-L, Ziobro M, et al. First-line pembrolizumab (pembro) monotherapy for advanced non-clear cell renal cell carcinoma (nccRCC): Results from KEYNOTE-427 cohort B. *J Clin Oncol*. 2019;37(7_suppl):546-546.

47. Atkins MB, McDermott DF, Powles T, et al. IMmotion150: A phase II trial in untreated metastatic renal cell carcinoma (mRCC) patients (pts) of atezolizumab (atezo) and bevacizumab (bev) vs and following atezo or sunitinib (sun). *J Clin Oncol*. 2017;35(15_suppl):4505-4505.

48. Rini BI, Powles T, Atkins MB, et al. Atezolizumab plus bevacizumab versus sunitinib in patients with previously untreated metastatic renal cell carcinoma (IMmotion151): a multicentre, open-label, phase 3, randomised controlled trial. *Lancet*. 2019;393(10189):2404-2415.

49. McGregor BA, McKay RR, Braun DA, et al. Results of a multicenter phase II study of

atezolizumab and bevacizumab for patients with metastatic renal cell carcinoma with variant histology and/or sarcomatoid features. *J Clin Oncol*. 2020;38(1):63-70.

50. Motzer RJ, Penkov K, Haanen J, et al. Avelumab plus Axitinib versus Sunitinib for Advanced Renal-Cell Carcinoma. *N Engl J Med*. 2019;380(12):1103-1115.

51. Baine MK, Turcu G, Zito CR, et al. Characterization of tumor infiltrating lymphocytes in paired primary and metastatic renal cell carcinoma specimens. *Oncotarget*. 2015;6(28):24990-25002.

52. Yuan C, Liu Z, Yu Q, et al. Expression of PD-1/PD-L1 in primary breast tumours and metastatic axillary lymph nodes and its correlation with clinicopathological parameters. *Sci Rep*. 2019;9(1).

53. Callea M, Albiges L, Gupta M, et al. Differential expression of PD-L1 between primary and metastatic sites in clear-cell renal cell carcinoma. *Cancer Immunol Res*. 2015;3(10):1158-1164.

54. Motzer RJ, Rini BI, McDermott DF, et al. Nivolumab for metastatic renal cell carcinoma: Results of a randomized phase II trial. *J Clin Oncol*. 2015;33(13):1430-1437.

55. Pignon JC, Jegede O, Shukla SA, et al. Irrecist for the evaluation of candidate biomarkers of response to nivolumab in metastatic clear cell renal cell carcinoma: Analysis of a phase II prospective clinical trial. *Clin Cancer Res*. 2019;25(7):2174-2184.

56. Thompson RH, Kuntz SM, Leibovich BC, et al. Tumor B7-H1 is associated with poor prognosis in renal cell carcinoma patients with long-term follow-up. *Cancer Res*.

2006;66(7):3381-3385.

57. Tykodi SS. PD-1 as an emerging therapeutic target in renal cell carcinoma: Current evidence. *Onco Targets Ther*. 2014;7:1349-1359.

58. George DJ, Hessel C, Halabi S, et al. Cabozantinib Versus Sunitinib for Untreated Patients with Advanced Renal Cell Carcinoma of Intermediate or Poor Risk: Subgroup Analysis of the Alliance A031203 CABOSUN trial. *Oncologist*. 2019;24(11):1497-1501.

59. Choueiri T, Escudier B, Powles T, et al. Cabozantinib versus Everolimus in Advanced Renal-Cell Carcinoma. *N Engl J Med*. 2015;373(19):1814-1823.

60. Flaifel A, Xie W, Braun DA, et al. PD-L1 Expression and Clinical Outcomes to Cabozantinib, Everolimus, and Sunitinib in Patients with Metastatic Renal Cell Carcinoma: Analysis of the Randomized Clinical Trials METEOR and CABOSUN. *Clin Cancer Res*. 2019;25(20):6080-6089.

61. Choueiri TK, Flaifel A, Xie W, et al. PD-L1 status and clinical outcomes to cabozantinib, sunitinib and everolimus in patients with metastatic clear-cell RCC treated on CABOSUN and METEOR clinical trials. *Ann Oncol*. 2018;29:viii726.

62. Wallin JJ, Bendell JC, Funke R, et al. Atezolizumab in combination with bevacizumab enhances antigen-specific T-cell migration in metastatic renal cell carcinoma. *Nat Commun*. 2016;7.

63. Powles T, Chowdhury S, Bower M, et al. The effect of sunitinib on immune subsets in metastatic clear cell renal cancer. *Urol Int*. 2011;86(1):53-59.

64. Adotevi O, Pere H, Ravel P, et al. A decrease of regulatory T cells correlates with overall survival after sunitinib-based antiangiogenic therapy in metastatic renal cancer patients. *J Immunother*. 2010;33(9):991-998.

65. Brauer MJ, Zhuang G, Schmidt M, et al. Identification and analysis of in vivo VEGF downstream markers link VEGF pathway activity with efficacy of anti-VEGF therapies. *Clin Cancer Res*. 2013;19(13):3681-3692.

66. Ruf M, Moch H, Schraml P. PD-L1 expression is regulated by hypoxia inducible factor in clear cell renal cell carcinoma. *Int J Cancer*. 2016;139(2):396-403.

67. Chevrier S, Levine JH, Zanotelli VRT, et al. An Immune Atlas of Clear Cell Renal Cell Carcinoma. *Cell*. 2017;169(4):736-749.e18.

68. Zajac AJ, Blattman JN, Murali-Krishna K, et al. Viral immune evasion due to persistence of activated T cells without effector function. *J Exp Med*. 1998;188(12):2205-2213.

69. Schraml P, Athelogou M, Hermanns T, Huss R, Moch H. Specific immune cell and lymphatic vessel signatures identified by image analysis in renal cancer. *Mod Pathol*. 2019;32(7):1042-1052.

70. Blackburn SD, Shin H, Haining WN, et al. Coregulation of CD8+ T cell exhaustion by multiple inhibitory receptors during chronic viral infection. *Nat Immunol*. 2009;10(1):29-37.

71. Kamphorst AO, Ahmed R. Manipulating the PD-1 pathway to improve immunity. *Curr Opin Immunol*. 2013;25(3):381-388.

72. Hargadon KM, Johnson CE, Williams CJ. Immune checkpoint blockade therapy for cancer: An overview of FDA-approved immune checkpoint inhibitors. *Int Immunopharmacol*. 2018;62:29-39.

73. Im SJ, Hashimoto M, Gerner MY, et al. Defining CD8+ T cells that provide the proliferative burst after PD-1 therapy. *Nature*. 2016;537(7620):417-421.

74. Sade-Feldman M, Yizhak K, Bjorgaard SL, et al. Defining T Cell States Associated with Response to Checkpoint Immunotherapy in Melanoma. *Cell*. 2018;175(4):998-1013.e20.

75. Siddiqui I, Schaeuble K, Chennupati V, et al. Intratumoral Tcf1 + PD-1 + CD8 + T Cells with Stem-like Properties Promote Tumor Control in Response to Vaccination and Checkpoint Blockade Immunotherapy. *Immunity*. 2019;50(1):195-211.e10.

76. Miller BC, Sen DR, Al Abosy R, et al. Subsets of exhausted CD8+ T cells differentially mediate tumor control and respond to checkpoint blockade. *Nat Immunol*. 2019;20(3):326-336.

77. Jansen CS, Prokhnevska N, Master VA, et al. An intra-tumoral niche maintains and differentiates stem-like CD8 T cells. *Nature*. 2019;576(7787):465-470.

78. Klatte T, Rossi SH, Stewart GD. Prognostic factors and prognostic models for renal cell carcinoma: a literature review. *World J Urol*. 2018;36(12):1943-1952.

79. Rini BI, Huseni M, Atkins MB, et al. Molecular correlates differentiate response to atezolizumab (atezo) + bevacizumab (bev) vs sunitinib (sun): Results from a phase III study (IMmotion151) in untreated metastatic renal cell carcinoma (mRCC). *Ann Oncol*.

2018;29:viii724-viii725.

80. Motzer RJ, Choueiri TK, McDermott DF, et al. Biomarker analyses from the phase III CheckMate 214 trial of nivolumab plus ipilimumab (N+I) or sunitinib (S) in advanced renal cell carcinoma (aRCC). *J Clin Oncol*. 2020;38(15_suppl):5009-5009.

81. Sharma S, Sharma MC, Sarkar C. Morphology of angiogenesis in human cancer: A conceptual overview, histoprognostic perspective and significance of neoangiogenesis. *Histopathology*. 2005;46(5):481-489.

82. Goddard JC, Sutton CD, Furness PN, Kockelbergh RC, O'Byrne KJ. A computer image analysis system for microvessel density measurement in solid tumours. *Angiogenesis*. 2002;5(1-2):15-20.

83. Nico B, Benagiano V, Mangieri D, Maruotti N, Vacca A, Ribatti D. Evaluation of microvascular density in tumors: Pro and contra. *Histol Histopathol*. 2008;23(5):601-607.

84. Ribatti D, Ennas MG, Vacca A, et al. Tumor vascularity and tryptase-positive mast cells correlate with a poor prognosis in melanoma. *Eur J Clin Invest*. 2003;33(5):420-425.

85. Nonomura N, Takayama H, Nishimura K, et al. Decreased number of mast cells infiltrating into needle biopsy specimens leads to a better prognosis of prostate cancer. *Br J Cancer*. 2007;97(7):952-956.

86. Strouch MJ, Cheon EC, Salabat MR, et al. Crosstalk between mast cells and pancreatic cancer cells contributes to pancreatic tumor progression. *Clin Cancer Res*. 2010;16(8):2257-2265.

87. Elpek GÖ, Gelen T, Aksoy NH, et al. The prognostic relevance of angiogenesis and mast cells in squamous cell carcinoma of the oesophagus. *J Clin Pathol*. 2001;54(12):940-944.

88. Maurer M, Theoharides T, Granstein RD, et al. What is the physiological function of mast cells? Introduction. *Exp Dermatol*. 2003;12(6):886.

89. Galli SJ, Tsai M, Wershil BK, Tama SY, Costa JJ. Regulation of mouse and human mast cell development, survival and function by stem cell factor, the ligand for the c-kit receptor. *Int Arch Allergy Immunol*. 1995;107(1-3):51-53.

90. Gurish MF, Austen KF. Developmental Origin and Functional Specialization of Mast Cell Subsets. *Immunity*. 2012;37(1):25-33.

91. Huang B, Lei Z, Zhang GM, et al. SCF-mediated mast cell infiltration and activation exacerbate the inflammation and immunosuppression in tumor microenvironment. *Blood*. 2008;112(4):1269-1279.

92. Norrby K, Jakobsson A, Sörbo J. Mast-cell secretion and angiogenesis, a quantitative study in rats and mice. *Virchows Arch B Cell Pathol Incl Mol Pathol*. 1989;57(1):251-256.

93. Tth T, Tth-Jakatics R, Jimi S, Takebayashi S, Kawamoto N. Cutaneous malignant melanoma: Correlation between neovascularization and peritumor accumulation of mast cells overexpressing vascular endothelial growth factor. *Hum Pathol*. 2000;31(8):955-960.

94. Blair RJ, Meng H, Marchese MJ, et al. Human mast cells stimulate vascular tube formation. Tryptase is a novel, potent angiogenic factor. *J Clin Invest*. 1997;99(11):2691-2700.

95. Kinet JP. The essential role of mast cells in orchestrating inflammation. *Immunol Rev*.

2007;217(1):5-7.

96. Saleem SJ, Martin RK, Morales JK, et al. Cutting Edge: Mast Cells Critically Augment Myeloid-Derived Suppressor Cell Activity. *J Immunol*. 2012;189(2):511-515.

97. Rüger B, Dunbar PR, Hasan Q, et al. Human mast cells produce type VIII collagen in vivo. *Int J Exp Pathol*. 1994;75(6):397-404.

98. Ribatti D. Mast cells and macrophages exert beneficial and detrimental effects on tumor progression and angiogenesis. *Immunol Lett*. 2013;152(2):83-88.

99. Eddy AA. Mast cells find their way to the kidney. *Kidney Int*. 2001;60(1):375-377.

100. Saruta T, Kondo K, Ohguro T, Ozawa Y, Kato E. Mast cells in human kidney cortex. *Keio J Med*. 1977;26(3):163-169.

101. Guldur ME, Kocarslan S, Dincoglu D, Ilyas Ozardali H, Ciftci H, Gumus K. The relationship of mast cells and angiogenesis with prognosis in renal cell carcinoma. *J Pak Med Assoc*. 2014;64(3):300-303.

102. Tuna B, Yorukoglu K, Unlu M, Mungan MU, Kirkali Z. Association of Mast Cells with Microvessel Density in Renal Cell Carcinomas. *Eur Urol*. 2006;50(3):530-534.

103. Mohseni MG, Mohammadi A, Heshmat AS, Kosari F, Meysamie AP. The lack of correlation between mast cells and microvessel density with pathologic feature of renal cell carcinoma. *Int Urol Nephrol*. 2010;42(1):109-112.

104. Chen Y, Li C, Xie H, et al. Infiltrating mast cells promote renal cell carcinoma angiogenesis by modulating PI3K → AKT → GSK3β → AM signaling. *Oncogene*. 2017;36(20):2879-

2888.

105. De Palma M, Biziato D, Petrova T V. Microenvironmental regulation of tumour angiogenesis. *Nat Rev Cancer*. 2017;17(8):457-474.

106. Guo X, Zhai L, Xue R, Shi J, Zeng Q, Gao C. Mast cell tryptase contributes to pancreatic cancer growth through promoting angiogenesis via activation of angiopoietin-1. *Int J Mol Sci*. 2016;17(6).

107. Visciano C, Prevete N, Liotti F, Marone G. Tumor-Associated Mast Cells in Thyroid Cancer. *Int J Endocrinol*. 2015;2015.

108. Li H, Xiao Y, Li Q, et al. The allergy mediator histamine confers resistanceto immunotherapy in cancer patients via activationof the macrophage histamine receptor H1. *Cancer Cell*. November 2021.

109. Jilaveanu LB, Puligandla M, Weiss SA, et al. Tumor microvessel density as a prognostic marker in high-risk renal cell carcinoma patients treated on ECOG-ACRIN E2805. *Clin Cancer Res*. 2018;24(1):217-223.

110. Carrato Mena A, Grande Pulido E, Guillén-Ponce C. Understanding the molecular-based mechanism of action of the tyrosine kinase inhibitor: Sunitinib. *Anticancer Drugs*. 2010;21(SUPPL.1):3-11.

111. Voce P, D'Agostino M, Moretti S, et al. Sunitinib inhibits tumor vascularity and growth but does not affect Akt and ERK phosphorylation in xenograft tumors. *Oncol Rep*. 2011;26(5):1075-1080.

112. Bhatt RS, Wang X, Zhang L, et al. Renal cancer resistance to antiangiogenic therapy is delayed by restoration of angiostatic signaling. *Mol Cancer Ther*. 2010;9(10):2793-2802.

113. Comoglio PM, Trusolino L, Boccaccio C. Known and novel roles of the MET oncogene in cancer: A coherent approach to targeted therapy. *Nat Rev Cancer*. 2018;18(6):341-358.

114. Gay CM, Balaji K, Byers LA. Giving AXL the axe: Targeting AXL in human malignancy. *Br J Cancer*. 2017;116(4):415-423.

115. Zhou L, Liu XD, Sun M, et al. Targeting MET and AXL overcomes resistance to sunitinib therapy in renal cell carcinoma. *Oncogene*. 2016;35(21):2687-2697.

116. Liu H, Sun S, Wang G, et al. Tyrosine Kinase Inhibitor Cabozantinib Inhibits Murine Renal Cancer by Activating Innate and Adaptive Immunity. *Front Oncol*. 2021;11(April):1-15.

117. Fu H, Zhu Y, Wang Y, et al. Tumor Infiltrating Mast Cells (TIMs) Confers a Marked Survival Advantage in Nonmetastatic Clear-Cell Renal Cell Carcinoma. *Ann Surg Oncol*. 2017;24(5):1435-1442.

118. Komi DEA, Redegeld FA. Role of Mast Cells in Shaping the Tumor Microenvironment. *Clin Rev Allergy Immunol*. 2020;58(3):313-325.

Acknowledgments of research support for the study: This work was supported by R21 CA238053-01, Dana-Farber / Harvard Cancer Center Kidney Cancer SPORE (P50-CA101942-12), and Exelixis Inc. T.K.C. is supported in part by the Kohlberg Chair at Harvard Medical School and the Trust Family, Michael Brigham, and Loker Pinard Funds for Kidney Cancer Research at DFCI.